An Integrative Simulation Model Linking Major Biochemical Reactions of Actin-Polymerization to Structural Properties of Actin Filaments

Aliaksandr A. Halavatyi, Petr V. Nazarov, Sandrine Medves, Marleen van Troys, Christophe Ampe, Mikalai Yatskou, Evelyne Friederich

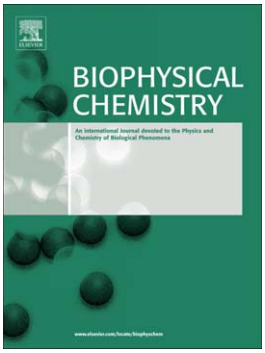

An Integrative Simulation Model Linking Major Biochemical Reactions of Actin-Polymerization to Structural Properties of Actin Filaments

Aliaksandr A. Halavatyi, Petr V. Nazarov, Sandrine Medves, Marleen van Troys, Christophe Ampe, Mikalai Yatskou, Evelyne Friederich

PII: S0301-4622(08)00237-8
DOI: doi: 10.1016/j.bpc.2008.11.006
Reference: BIOCHE 5186

To appear in: *Biophysical Chemistry*

Received date: 16 September 2008
Revised date: 10 November 2008
Accepted date: 11 November 2008

Please cite this article as: Aliaksandr A. Halavatyi, Petr V. Nazarov, Sandrine Medves, Marleen van Troys, Christophe Ampe, Mikalai Yatskou, Evelyne Friederich, An Integrative Simulation Model Linking Major Biochemical Reactions of Actin-Polymerization to Structural Properties of Actin Filaments, *Biophysical Chemistry* (2008), doi: 10.1016/j.bpc.2008.11.006

An Integrative Simulation Model Linking Major Biochemical Reactions of Actin-Polymerization to Structural Properties of Actin Filaments

Aliaksandr A. Halavatyi[*,#,⊥], Petr V. Nazarov[*,†,⊥], Sandrine Medves[#], Marleen van Troys[§,&], Christophe Ampe[§,&], Mikalai Yatskou[#,†], Evelyne Friederich[#,†,1]

[*] Department of Systems Analysis, Belarusian State University, 4, Nezavisimosti Ave, 220030 Minsk, Belarus

[#] Faculty of Sciences, Technology and Communication, Life Sciences Research Unit, University of Luxembourg, 162 A, avenue de la Faïencerie, L-1511 Luxembourg, Luxembourg

[†] Centre de Recherche Public Santé, 84, Rue Val Fleuri, L-1526 Luxembourg, Luxembourg

[§] VIB Department for Molecular Biomedical Research, UGent, VIB, A. Baertsoenkaai 3, Gent, Belgium

[&] Department of Biochemistry, Faculty of Medicine and Health Sciences, UGent, A. Baertsoenkaai 3, Gent, Belgium

[⊥] These authors contributed equally to this work

[1] Author to whom correspondence should be addressed at University of Luxembourg, Faculty of Sciences, Technology and Communication, 162 A, avenue de la Faïencerie L-1511 Luxembourg

Office address: Campus Limpertsberg, 162 A, avenue de la Faïencerie, L-1511 Luxembourg

Telephone: +352 46 66 44 6645

E-mail: evelyne.friederich@uni.lu

Pages: 33, **Tables:** 1, **Figures:** 5.

Abbreviations used

F-actin	Filamentous actin
nSRF model	non-structurally-resolved filament model
SRF model	structurally-resolved filament model
Pi	Phosphate
ATM	Globular actin (monomeric form) with incorporated ATP
ADM	Globular actin (monomeric form) with incorporated ADP
ATF	Filamentous actin protomer (F-actin) with incorporated ATP
APF	Filamentous actin protomer (F-actin) with incorporated ADP-Pi
ADF	Filamentous actin protomer (F-actin) with incorporated ADP
FTB	Barbed ends of filaments, terminating by ATP-actin
FPB	Barbed ends of filaments, terminating by ADP-Pi-actin
FDB	Barbed ends of filaments, terminating by ADP-actin
FTP	Pointed ends of filaments, terminating by ATP-actin
FPP	Pointed ends of filaments, terminating by ADP-Pi-actin
FDP	Pointed ends of filaments, terminating by ADP-actin
CBM	Barbed-end capping protein (capper) in monomer (free) form
CBF	Barbed-end capper bound to filament
CPM	Pointed-end capper in monomer (free) form
CPF	Pointed-end capper bound to filament
FOM	Formin in monomer (free) form
FOF	Formin, bound to filament barbed ends
ARM	Arp2/3 complex in monomer (free) form
ARF	Arp2/3 complex associated with filament
FRP	Arp2/3 complex associated with filament pointed end (pointed ends of filaments, terminating by ARP2/3 complexes)
FRB	Arp2/3 complex associated with filament with no bound actins (barbed ends of filaments, terminating by ARP2/3 complexes)

Abstract

We report on an advanced universal Monte Carlo simulation model of actin polymerization processes offering a broad application panel. The model integrates major actin-related reactions, such as assembly of actin nuclei, association/dissociation of monomers to filament ends, ATP-hydrolysis via ADP-Pi formation and ADP-ATP exchange, filament branching, fragmentation and annealing or the effects of regulatory proteins. Importantly, these reactions are linked to information on the nucleotide state of actin subunits in filaments (ATP hydrolysis) and the distribution of actin filament lengths. The developed stochastic simulation modelling schemes were validated on: i) synthetic theoretical data generated by a deterministic model and ii) sets of our and published experimental data obtained from fluorescence pyrene-actin experiments. Build on an open-architecture principle, the designed model can be extended for predictive evaluation of the activities of other actin-interacting proteins and can be applied for the analysis of experimental pyrene actin-based or fluorescence microscopy data. We provide a user-friendly, free software package *ActinSimChem* that integrates the implemented simulation algorithms and that is made available to the scientific community for modelling *in silico* any specific actin-polymerization system.

Key words: Actin; Filament; Polymerization; Model; Monte Carlo simulation; Software.

1. Introduction

Actin is a protein capable of self-assembling into dynamic filaments that form the actin cytoskeleton. This process is required for many crucial physiological functions like morphogenesis, cell migration and division or cell communication. In cells, actin monomer assembly and filament organization are controlled in time and space by associated proteins [1-4]. Because of its essential functions in cells, it is not surprising that perturbations of the actin cytoskeleton are associated with numerous diseases, including cancer, myopathies- and neurodegenerative disorders. For example, uncontrolled migration of cancer cells leads to metastasis and is significantly dependent on perturbed actin polymerization [5, 6]. In addition, several pathogens, like *Listeria monocytogenes*, use actin polymerization for their propulsion inside infected cells [7, 8]. Thus, a thorough understanding of how actin polymerization is regulated to generate forces and movement will lead to a better understanding of how it contributes to these physio-pathological processes [9].

Many biophysical models have been proposed for the mechanisms by which actin filament assembly generates force that is translated into movement (see [10] for review). In addition, specific biochemical models were established to evaluate the effects of regulatory proteins on the actin polymerization reaction such as nucleation and filament elongation in the presence of formins [11-13] or the Arp2/3 complex [14-16], effects of capping [14, 17, 18], or of severing proteins [19-21]. These deterministic models rely on solving differential equations. One of the efficient non-analytical approaches which in principle can describe the actin polymerization processes is the Monte Carlo simulation [22]. Obviously, stochastic Monte Carlo models have a considerable potential because: i) they can describe adequately many actin-polymerization processes simultaneously, such as spontaneous or stimulated actin nucleation, (un)branching, fragmentation, annealing, complete depolymerisation, (un)capping, two-step ATP-hydrolysis [18, 23]; ii) in addition stochastic models have the advantage that they can be applied to complex situations involving structural information and distribution of actin filament lengths [24, 25]. Moreover, Monte Carlo models are easy to understand, since the simulation algorithms are made from so-

called first principles known on the studied systems, and not requiring a strong mathematical background [26, 27]. However, so far, no comprehensive universal Monte Carlo model and software of actin-polymerization reactions with a broad application panel for various actin polymerization processes are available.

In this paper, we developed a systematic Monte Carlo simulation formalism and an computational tool for modelling and analysing the main actin polymerization reactions, uniquely including the nucleotide compositions of monomers and filaments, and the distribution of actin filament lengths. This tool was evaluated using well-characterized reactions such as actin association to and dissociation from filaments, assembly of actin nuclei (spontaneous and stimulated by capping-proteins or formin), filament capping-related reactions, ATP-hydrolysis and ATP recharge of actin monomers, filament branching, fragmentation and annealing. The simulation models and computational algorithms were integrated in the stand-alone executable software package *ActinSimChem*.

2. Model

2.1. The model formalism

Actin polymerization is used by cells as a source of mechanical forces, which can be translated into cell propulsion. The process of actin assembly is influenced by the concentration of monomeric actin charged with ATP or ADP nucleotide, physical and biochemical conditions and, importantly, by different actin-regulatory proteins: actin nucleators such as the Arp 2/3 complex and formin, different end cappers and severing proteins like cofilins [9]. In this work, we considered the reactions between ATP- and ADP-actin monomers (ATM, ADM, *cf*. the section Abbreviations used), formin (FOM, a protein stimulating actin monomer assembly), actin nucleator Arp 2/3 complex (ARM), and end cappers (CBM, CPM, regulating actin filament dynamics at barbed (B) or pointed (P) ends). Kinetic actin polymerization experiments have shown that capping proteins also nucleate actin polymerization in the presence of excess actin ATP-monomers [28].

Diagrams, showing the formalization of actin polymerization processes, are given in Fig. 1. Actin monomers self-assemble to form trimers with the rate constant k_{SNUC}. Actin filaments grow from these "nuclei" by addition of monomers. The structural asymmetry of the filament ends is correlated with dissimilar assembly and disassembly rates. An actin filament grows under appropriate conditions approximately ten times faster at the barbed end than at its pointed end. The growing process is reversible and it is controlled by a polymerization-depolymerization equilibrium. The aging of F-actins occurs when ATP hydrolyses with the rate constants k_{TTOP} and k_{PTOD} via the ADP-Pi "intermediate" state, consisting in ADP with a weakly associated phosphate. ATP hydrolysis results in weakening of actin subunit interaction and destabilization of the actin filament. Free ADP-actin monomers exchange their nucleotide for ATP because of the higher affinity of monomeric actin for ATP [29]; we introduced here the rate constant k_{DTOT} to describe this process.

Free ends of a filament can be reversibly capped by either barbed or pointed end cappers. Capping proteins or formin promote actin nucleation, mostly by stabilizing actin trimers, at much higher rates ($k_{CBNU,}$ k_{CPNU} and k_{FNUC}) when compared to the rate of spontaneous actin nucleation (k_{SNUC}). In addition, formin being attached to the barbed end of nucleated actin oligomers, can significantly speed up barbed end elongation of the filament [11]. Branching reactions of Arp2/3 complex with F-actins are realized according to the mechanism of side branching [14]. The reactions of filament fragmentation and annealing were integrated as reported in [25]. We assume spontaneous fragmentation occurs in a manner invariant to position and nucleotide state of the actin-protomer (the rate constant k_{FRGM}). Annealing reaction consists in adhesion of free barbed ends and pointed ends of filaments with the rate constant k_{ANNL}. Other hypotheses on mechanisms of filament branching, fragmentation, annealing, nucleation, capping, can accordingly also be integrated within the frame of our simulation scheme.

To build the simulation model for actin polymerization we made the following assumptions:

- Actin-polymerization is simulated in a cubic volume of the size V with periodic boundary conditions.

- Since free actin monomers and free actin-associated proteins (cappers, Arp2/3, formins) diffuse rapidly [30-33], we assumed their spatial distribution is homogeneous.
- Quantities of monomeric proteins, i.e. the numbers of molecules $N_{ATM,}$ $N_{CBM,}$ *etc.* in the volume *V*, are calculated from the initial molecular concentrations $[ATM]_{t=0}$, $[CBM]_{t=0}$, etc.
- Filaments are simulated as independent objects.
- The total concentrations of the monomeric proteins are constant over the volume *V*.

The flow diagram of the developed integrative stochastic simulation model of actin polymerization processes is shown in Fig. 2A. The core of this model is the ability to reproduce any complex actin polymerization system in a unique and universal way, whatever particular actin-based system is used. It combines various molecular reagents, chemical reactions and structures of actin filaments within a unique stochastic simulation scheme (Fig. 2B). The integrity of this modelling approach is based on an open-architecture principle, allowing easy incorporation of new reagents, additional actin-polymerization reactions, filament structures or even new stochastic simulation algorithms.

Presently, to simulate actin polymerization processes, we used n_R = 21 molecular reagents participating in M = 28 chemical actin-related reactions (*cf.* Table 1). Reagents are globular and filamentous actins (with incorporated ATP/ ADP-Pi/ADP nucleotide), barbed and pointed ends of filaments (terminated by ATP-/ADP-Pi-/ADP-actins), barbed and pointed end capping proteins, formin and the Arp2/3 complex (either as free forms or associated with filaments). The filaments are represented as consequences of protomer associations characterised by the number of protomers, the nucleotide states of these protomers, the number and types of pointed and barbed ends, pointers to filamentous ends and actin related proteins, branching units, i.e. the sites for growth of ‘daughter’ branches. Any daughter branches to a ‘mother’ filament are similarly organised.

2.2. The simulation of reactions

To simulate the chemical interactions between molecular reagents in the actin filaments a proper discrete-event Monte Carlo simulation methodology is needed. Several stochastic simulation strategies have been implemented and compared. More specifically, we developed new simulation schemes based on the updates of the Gillespie's "direct" method and its modifications: the “first reaction” method [34], the "next reaction" method of Gibson-Bruck [35] and the τ-leap algorithm [36]. The best results were obtained for the one generated on the base of the Gillespie's "direct" algorithm [see **Supplementary material**]. A flow diagram of the stochastic simulation scheme implemented in our model is shown in Fig. 2B.

The simulation starts in **block 1** by setting the volume V, the initial numbers of molecules $\mathbf{N} = (N_{ATM}, N_{ADM}, \ldots, N_{FRB})$, and the rate constants $\mathbf{K} = (k_{SNUC}, k_{CBNU}, \ldots, k_{DTOT})$. In **block 2** the concentration-dependent reaction rates a_i, where i is the index running for 28 reactions {*SNUC*, *CBNU*, …, *DTOT*} (*cf.* Table 1), are calculated using Eq. (1) or Eq. (2).

$$a_i = k_i \left(10^{-6} N_A V\right)^{1-n_i} \prod_{j=1}^{n_i} N_j \,, \tag{1}$$

where

n_i is the number of reagents participating in the i-th reaction;

k_i is the experimental concentration-independent rate constant, given in the same units as in Table 1 (s^{-1}, $\mu M^{-1}s^{-1}$, $\mu M^{-2}s^{-1}$, and $\mu M^{-3}s^{-1}$ for n = 1, 2, 3, and 4 respectively);

N_A is the number of Avogadro;

N_j is the number of molecules of j-th type, contained in volume V. This number is linked with the concentration of the j-th reagent as $C_j = N_j/V$.

Eq. (1) is applied if only one molecule of each reacting reagent is simulated in the i-th reaction. If more than one molecule of at least one reagent participates in the reaction, as, for instance, in the formin-initiated nucleation, then Eq. (2) can be calculated based on an analogy with [37].

$$a_i = k_i \left(10^{-6} N_A V\right)^{1-\eta_i} \prod_{j=1}^{n_i} \left(\prod_{l=1}^{m_i{}^j} \left(N_j - l + 1\right) \right) \tag{2}$$

where

m_i^j is the number of molecules of *j-th* reagent, required for occurrence of *i*-th reaction.

$\eta_i = \sum_{j=1}^{n_i} m_i{}^j$ is the total number of molecules, participating in the *i*-th reaction. For instance for the formin-initiated nucleation $n_{FNUC} = 2$ (ATM and FOM are the reagents for this reaction), $m_{FNUC}{}^{ATM} = 3$, $m_{FNUC}{}^{FOM} = 1$ and $\eta_{FNUC} = 4$.

The selection of the type of the next reaction is performed in **block 3** using a random number generator so that the probability to select *r*-th reaction is proportional to the value of a_r, where *r* is the index running for 28 reactions {*SNUC, CBNU, …, DTOT*}.

The time towards the reaction τ is calculated in **block 4**, using an assumption that the flow of reaction-events is a Poisson flow [34], and, therefore, the times between events are exponentially distributed. Using the method of inverse functions, the time τ can be calculated as

$$\tau = -\left(\sum_i a_i\right)^{-1} \ln(\xi) \tag{3}$$

where ξ is the uniformly distributed random number from the interval (0,1).

The *f*-th filament, to which the reaction will be applied, is randomly selected among the total number n_F of filaments in **block 5** using a new realization of a random number generator. The filament selection procedure is a numeric routine governed by a complex density probability function of the numbers of branches, pointed and barbed ends for the current state of filaments distribution. If the annealing reaction is gambled then two new random numbers are generated. This step is not needed in case of the nucleation reactions.

In **block 6** the *p*-th filamentous unit in the *f*-th filament is generated, using a new realization of a random number generator, on which a reaction either of hydrolysis, branching, or fragmentation occurs. This step is ignored in case of nucleation, association, dissociation, capping, uncapping, annealing reactions.

The reaction is performed in **block 7** in accordance with a formal scheme listed in Table 1. Each reaction results in a modification of the number of molecules and structure of one of the filaments. Exceptions to this are the hydrolysis and recharging reactions, which affect only structure of proteins. Nucleation and fragmentation reactions result in appearance of new filaments. Annealing reaction leads to the disappearance of one of the filaments. Branching reaction yields a new filament branch. When one type of the actin-monomer dissociation reactions occurs, the length of the filament is checked. If it contains less then 3 actin protomers – the filament dissociates, releasing all attached proteins (i.e. formin, capping proteins). The ATP-related type of F-actin ends (FTB, FDB, FTP, FDP) can be changed after association and dissociation reactions.

Finally, the systems time t is increased by τ (**block 8**), and if the simulation time is less than the predefined maximal simulation time t_{max} (**block 9**), the algorithm returns to block 2. Otherwise simulation stops in **block 10**, providing a list of output characteristics, i.e. evolution of concentrations in time, the distribution of filament lengths, and actin nucleotide states in filaments.

2.3. Non-structurally-resolved filament (nSRF) and structurally-resolved filament (SRF) models

We developed two variants of structural representations of actin filaments: the non-structurally-resolved filament (nSRF) model and the structurally-resolved filament (SRF) model.

In the nSRF model a filament is represented by the number of ATP-containing actins (ATF), the number of ADP-Pi-containing actins (APF), the number of ADP-containing actins (ADF) and by type and state of the barbed and pointed ends. Selection of the state of actins (ATF/APF/ADF) bound to filament ends is performed as follows. The state of a last attached protein is stored in a model parameter called as "state of barbed/pointed end". It thus defines the states of the corresponding ends of the filament, i.e. FTB/FTP, FPB/FPP, FDB/FDP, FRB/FRP, CBF/CPF, or FOF. After dissociation of a monomer from the filament, the state of the next filament bound-actin monomer, that will define a new type of end, is selected preferably from ATF actins. If no ATF actins are left, the filament end switches into ADP-Pi- (preferably) or ADP-related form. The SRF model is similar to the nSRF model but is additionally represented by the bidirectional list of actin

types (ATF/APF/ADF) and actin-accessory proteins (CBF/CPF/FOF/ARF), which defines mutual positions of protomers in the filament. During filament growth, a marker is stored in the bidirectional list to define ATP/ADP-Pi/ADP-state of each actin or subunit and/or actin-associated protein in filament. The list has two access points – pointers to the barbed and pointed ends. This organization permits swift addition/removal of monomers at the ends and splitting/merging of lists for fragmentation/annealing reactions. When Arp2/3 induced-branching is included, the pointers to 'mother' and 'daughter' filament branches are stored in the SRF and nSRF models. The SRF model also stores positions of attachment points on the 'mother' filament or branch regarding the pointed end.

Using the SRF model is more time-consuming due to processing the bidirectional list. The nSRF model is aimed to speed up the simulation by simplifying the representation of filaments. The SRF model is more accurate than the nSRF model and, by accounting for mutual positions of ATP- and ADP-actins in filaments as described above, it gives a powerful opportunity for the evaluation of nucleotide compositions without any restrictions and conditions imposed on the distribution of filament lengths. By using the SRF model one is additionally able to check: (i) depolymerization of preformed actin filaments networks, (ii) filament severing, for example, by cofilins, which have a higher affinity for ADP-actin [38], (iii) other polymerization processes taking in account the nature of the nucleotide such as the Arp2/3 association and side branch initiation which is preferable occurring at an ATP-charged protomer.

2.4. Error analysis

Stochastic deviations in the simulated results, yielding asymptotic solutions of the investigated processes, are inherent to the Monte Carlo simulation technique. In addition, powerful computational facilities are required. Increasing a volume V and averaging the results of n_A independent simulations help to reduce the stochastic deviation. Therefore, we developed a verification rule for an optimal selection of the simulation volume V and the number of averaging n_A (see **Supplementary material**). An increase of n_A is preferable over an increase of V. The latter

has a bottom cut-off to avoid any discontinuity at low concentrations and rare reactions. We estimated a possibly minimal volume needed for analysis of actin polymerization processes. Assume that the minimal number of reacting molecules is equal to 20. If the minimal initial concentration of a reagent is 1 nM then the minimal volume becomes $V_{min} \approx 33$ μm^3. If the polymerization starts from a low-rate nucleation with the rate constant of ~10^{-9}–10^{-8}, the selection of a larger volume of $V > 125$ μm^3 may, however, be required.

3. Additional experimental procedures

The developed models were evaluated for analysis of experimental data from fluorescence pyrene-actin polymerization assays. Below we used data reported in literature [14] or generated as described in 3.1.

3.1. Actin polymerization assays using proteins purified from tissues or produced in E. coli

Actin was prepared from rabbit skeletal muscle [39] and further purified using Sephacryl S-300 (Pharmacia) in G-buffer [5 mM Tris-HCl, pH 7.7, 0.1 mM $CaCl_2$, 0.2 mM ATP, 0.2 mM dithiothreitol (DTT), 0.01% NaN_3]. Actin was labelled with Pyrene on Cys374 following Kouyama and Michashi [40]. To produce recombinant formin FH1-FH2 domain, the corresponding mouse formin cDNA (mDia-1) was cloned into the pQE30 vector (Qiagen). The production of the His tagged-FH1-FH2 domains was carried overnight at 16°C, after induction with 1 mM IPTG. Proteins were purified from bacterial lysates using Talon® Metal Affinity Resin (Clontech) and eluted by 500 mM Imidazole. The His tagged-FH1-FH2 protein was dialysed against 100 mM Tris pH 7.5; 100 mM KCl; 1mM DTT.

Polymerization of pure actin (3 or 2 μM, 20% pyrene-labeled, in G-buffer) or actin in the presence of formin, was induced by addition of KCl and $MgCl_2$ to final concentrations of 100 and 1 mM, respectively. The fluorescence increase, proportional to filament formation, was followed as function of time using a F-4500 fluorimeter (Hitachi) (excitation at 365 nm and emission at 388 nm). Experimentally obtained fluorescence data were corrected for background fluorescence by

subtraction of the constant, equal to fluorescence at t = 0 s. Subsequently, the fluorescence units were rescaled, to fit simulated concentrations. Several studies have shown that the pyrene fluorescence intensity of ADP F-actin is substantially stronger than that of ATP F-actin [23, 41]. Consequently the relative amounts of ATP F-actin and ADP F-actin has been included in correlating pyrene intensity and F-actin concentration. In this work, the best quality of fit to experiments, giving the minimum error (**Supplementary material**, Eq. B1), was obtained for a ratio of 0.5 of F-ATP to F-ADP-actin.

3.2. Model validation

First, the source code was verified (see **Supplementary material**). Second, we tested and validated the Monte Carlo model by comparison with synthetic theoretical data. A system of corresponding differential equations was used for a number of pre-selected sets of biochemical parameters published elsewhere. Third, we compared the computational efficiency and agreement of various actin filament models: non-structurally-resolved (nSRF) and structurally-resolved filament (SRF) models. Finally, we applied our model for the analysis of pyrene-actin based fluorescence actin-polymerization experiments: i) actin polymerization, ii) actin polymerization in the presence of actin-capping protein [14], or iii) formin.

4. Results and discussion

4.1. Strategy for model evaluation and analysis

We evaluated the performance of the developed models on well-characterized theoretical and published data. We considered fundamental reactions including monomer assembly into filaments, filament end capping and assembly of actin oligomer nuclei by capping protein or formin. The complete list of the reactions events simulated is shown in Fig. 1. Our simulations are performed for V =125 μm^3 and n_A =50. For computational reasons and taking into account its minor effect on the systems considered in our tests we do not include in the simulations the reactions associated with the ADP-Pi “intermediate” nucleotide state. Instead, we approximated the filament aging reaction

(hydrolysis of ATP in filaments) with the overall rate constant 0.0007 s^{-1}, which is assumed to be a lowest limit for an approximative two-step hydrolysis rate constant (including phosphate release), and is a product of rate constants for hydrolysis 0.3 s^{-1} [42] and phosphate release 0.0026−0.004 s^{-1} [43, 44].

We compared the nSRF model with a deterministic kinetic model for the simplest situation, in which the behaviour of the actin system can be described by a system of differential equations. Such deterministic models have been used to describe actin polymerization kinetics (see e.g. [13, 14, 45, 46]). Subsequently, we compared and evaluated simulations obtained with the SRF and nSRF models, a key step towards the model validation. First, agreement between two independently implemented models gives a good confidence that no technical or logical errors were made during programming of the modelling algorithms. Second, this comparison helps to investigate the application range of the nSRF model, i.e. to determine when the simplifications of the nSRF model are acceptable and do not lead to significant changes in simulation results. Finally, to further evaluate the robustness of the developed models, we applied the simulation models to some selected experimental data and evaluated how reagents affect the reactions.

4.2. Evaluation of the developed models by analytical solutions

4.2.1. Polymerization reaction of actin

Actin assembly is a simple model system. The concentration of F-actin only slowly increases in the early phase (the so-called *lag phase*) due to slow spontaneous nucleation. Then a period of fast elongation follows, during which the concentration of F-actin increases more rapidly. Consequently globular actin decreases and asymptotically approaches to the so-called critical concentration C_c. The critical concentration, which is independent from the initial actin concentration, can be calculated via association/dissociation rates, Eq. (4).

$$C_c = (k_{DITB} + k_{DITP}) / (k_{ASTB} + k_{ASTP}) \quad (4)$$

We initially assume that no ATP-hydrolysis occurs in a system, i.e. no aging of F-actins, and, thus, only ATM and ATF actins exist in this system. This assumption is needed to build the system of the

analytical equations (see **Supplementary material**) and not a limitation linked to the presented simulation (see 4.3.1). The rate constants (for references see Table 1) used in modelling are: k_{SNUC} = 10^{-8} $\mu M^{-2}s^{-1}$, k_{ASTB} = 11.5 $\mu M^{-1}s^{-1}$, k_{ASTP} = 1.3 $\mu M^{-1}s^{-1}$, k_{DITB} = 1.4 s^{-1}, k_{DITP} = 0.8 s^{-1}. The nSRF model was launched and tested at three initial actin concentrations $[ATM]_{t=0}$ = 3, 6 and 12 μM. Predicted F-actin concentrations obtained either by the nSRF model or by the analytical model (Eq. (C1), **Supplementary material**) for the actin systems with different actin concentrations are plotted in Fig. 3A and indicate a good agreement between simulated and analytical data.

4.2.2. Actin polymerization reaction in the presence of capping protein

Addition of barbed-end capping protein in the system above introduced two effects: i) increase of the nucleation rate and ii) inhibition of further elongation from the barbed end by capping. The analytical model for actin polymerization in the presence of a barbed-end capping protein was reported in [14] and briefly given in **Supplementary material** (Eq. (C2)). Again, no aging of F-actins is assumed (this is necessary to avoid tracking the ATP/ADP state of the ends for each separate filament). The numerical experiments were launched with the rate constants: k_{SNUC} = 10^{-8} $\mu M^{-2}s^{-1}$, k_{CBNU} = 10^{-5} $\mu M^{-3}s^{-1}$, k_{ASTB} = 11.5 $\mu M^{-1}s^{-1}$, k_{ASTP} = 1.3 $\mu M^{-1}s^{-1}$, k_{DITB} = 1.4 s^{-1}, k_{DITP} = 0.8 s^{-1}, k_{ASCB} = 3 $\mu M^{-1}s^{-1}$, k_{DICB} = 4 x 10^{-4} s^{-1} (*cf.* Table 1). Predicted concentrations of F-actin by the nSRF (circles, diamonds) and analytical model (lines) for the initial protein concentrations $[ATM]_{t=0}$ = 2 μM, and $[CBM]_{t=0}$ = 0.1, 0.01 μM are plotted in Fig. 3B. The fact that the results of simulated and analytical models of actin polymerization, with or without capping protein, are in good agreement validates the developed simulation model.

A broader range of examples and tests of the models is shown in **Supplementary material** (Fig. S1 – S2). Fig. S1 demonstrates that simulations that predict the average filament length and the filament length distribution at steady-state changed drastically in presence of fragmentation and annealing, in line with [25]. Fig. S2 shows a simulation of overshoot occurrence under various conditions of polymerization kinetics.

4.3. Comparison of the nSRF and SRF models

4.3.1. Polymerisation of actin in the absence of other proteins

A major difference between SRF and the nSRF model (and, *a fortiori*, previous analytical models) is, that the former inherently incorporates the possibility of aging of F-actin. This is now taken into account and simulated as a stochastic reaction with the rate constant 0.0007 s^{-1}. The SRF model combines information about type and position of each monomer in the filament, whereas in the nSRF model it is assumed that ATP-containing F-actins (ATF) are allocated near the filament ends, and ADP-actins (ADF) in the middle. The latter, rather rough approximation of the F-actin aging mechanism may result in biased models solutions, in particular for a time period longer than 1000 seconds, assuming a slow rate constant ~ 10^{-3} s^{-1} for the hydrolysis reaction.

Fig. 4A plots the predicted concentrations of F-actin resulting from the SRF (symbols) and nSRF (lines) models for three initial concentrations of actin $[ATM]_{t=0}$ = 3, 6 and 9 μM. The concentration of F-actin slowly increases in early phase, consistent with the experimentally observed *lag phase* (see e.g. Fig. 5B), due to slow spontaneous nucleation (k_{SNUC} =10^{-8} $\mu M^{-2}s^{-1}$). During fast elongation the concentration of F-actin increases, consequently globular actin decreases and asymptotically approaches the critical concentration C_c which here is 0.17 μM. Therefore, the concentration of F-actin asymptotically approaches values of 2.83, 5.83 and 8.83 μM (Fig. 4A).

During nucleation and elongation the rates of ADP-actin association and dissociation do not play an important role, because of fast ATP-actin recharge in the monomer pool and significant prevailing of the ATP-actin association reactions. At this stage no deviation can be detected when comparing both models, therefore the nSRF model can be used instead of SRF to predict systems behaviour in the non-equilibrium elongation phase of the filament. The simulation time required by the nSRF model for an actin system is about 30 times lower than that of the SRF model.

To evaluate the effect of ATP hydrolysis and filament aging, we varied the model parameters. We assumed that no actin recharge occurred and, to make the effect of aging more pronounced, we increased the aging rate up to one hundred times, and increased the rate of spontaneous nucleation

up to k_{SNUC} =10^{-6} $\mu M^{-2}s^{-1}$. Since the effect may appear only when association no longer prevails over dissociation, a long time period of t_{max} = 8000 s was considered. The simulation results of the system for $[ATM]_{t=0}$ = 2 μM are shown in Fig. 4B. No deviation was observed for the period of filament elongation, however, the subsequent late dissociation phase significantly differed for the two models. This deviation occurred even if actin ATP-recharge was switched on, however to a much lesser degree (data not shown).

This result indicates that when ATP-actin recharge exists in the system, the simplified nSRF model can be used during the periods of *lag-phase* and fast filament elongation. To further confirm this result, we considered more complex systems including actin regulatory proteins that cap or nucleate actin polymerization.

4.3.2. Actin polymerization reactions in the presence of end cappers or nucleating proteins

A barbed-end capping protein initially promotes assembly of oligomeric actin nuclei and subsequently inhibits elongation of the filament barbed end by remaining associated with it [14, 17] thereby it can affect the critical concentration. Previous reports on modelling of actin polymerization suggested that the nucleation reaction involves 6 actin monomers, without however excluding that nucleation with 3 monomers might be also possible [14]. We used 3 actin molecules and an attached capping protein as a filament nucleus for simplification (see reaction with the rate constant k_{CBNU} in Table 1).

Fig. 4C shows the results of the simulation for 3 μM actin in the presence of 0.01 or 0.1 μM barbed-end capping protein, respectively. The nucleation rate of the capping-protein was set to 10^{-5} $\mu M^{-3}s^{-1}$. Nucleation activity of the capping protein considerably increased the rate at which actin filaments formed, as a function of capping protein concentration. The steady-state F-actin concentration was, however, higher for lower capping protein concentration: 2.51 μM for $[CBM]_{t=0}$ = 0.01 μM vs. 2.41 μM for $[CBM]_{t=0}$ = 0.1 μM. No deviation could be observed between the results of SRF (symbols) and nSRF (lines) model for the time between 0 and 2000 s (Fig. 4C). For longer times slight deviations appeared (not shown), as observed for the system with actin alone.

Next, we analyzed the effect of pointed-end cappers at similar concentrations. We assumed that this protein had similar properties (including rate constants) as the barbed-end capping protein, with the difference that it attached to the pointed end of the filament. Fig. 4D revealed a good agreement between models. The time scale of the plot was between 0 and 1000 s, since, as was expected, the F-actin elongation rate was approximately 3 times faster than that in the presence of the barbed-end capping protein. Moreover, the steady-state concentrations of F-actin were around 2.9 μM (for both CPM concentrations) due to the difference in critical concentrations of monomeric actin for free barbed (~ 0.12 μM) and pointed (~ 0.61 μM) ends.

4.3.3. Formin-mediated effects on actin polymerization system

There are two main functions of formin in actin polymerization: it assembles actin and acts as a processive motor of filament elongation. In the presence of profilin, formin effectively generates long ADP-rich filaments, as was reported in [11]. The elongation rate in this situation may reach values of 110 $\mu M^{-1}s^{-1}$. In the absence of profilin, the elongation is less efficient, with a rate constant of 9 $\mu M^{-1}s^{-1}$ [12].

In our simulations we used the information from [11] and [13] to estimate formin-associated rate constants (see Table 1, reaction with rate constants k_{FNUC}, k_{FASB}, k_{DIFB}). The rate of spontaneous association of formin to a free barbed-end was put arbitrary, k_{ASFB} = 3 $\mu M^{-1}s^{-1}$, however, this reaction does not demonstrate a high influence on the polymerization, because usually all free formins tend to nucleate new filaments. The result of the comparison of SRF and nSRF models for a 2 μM actin assay is given in Fig. 4E. Note, that the time window of the simulation [0; 200 s] is very different from the previous situations and that the speed of filament growth has increased significantly. For both formin concentrations tested, the final F-actin concentration is equal to 1.997 μM, calculated as extrapolation to longer times, with almost all actin molecules in the F-form.

4.3.4. Effect of the full reaction set on actin polymerization system

We theoretically compared the simulation results for the condition in which all reagents and reactions are present (Table 1, Fig. 1). Selected initial concentrations are: [ATM] = 2 and 3 μM; $[CBM]_{t=0}$ = 0.01 μM, $[CPM]_{t=0}$ = 0.01 μM, $[FOM]_{t=0}$ = 0.001 μM, $[ARM]_{t=0}$=0.01 μM. This is a very complex situation since barbed end capping protein interferes with formin and formin lowers the binding of capping protein to barbed ends by 100 fold without, however, competing for barbed end binding ([11], supplement data on gelsolin). In addition, several reactions including the Arp2/3 dependent branching reaction, change the number of (barbed) filament ends. Despite this complexity, the comparison of F-actin behaviour for two tested actin concentrations shown in Fig. 4F, demonstrates that the results for SRF and nSRF models were in a good agreement. Using our model, we can in addition investigate an effect of the branching reaction, in terms of the relevant rate constant and the concentration of the Arp2/3 complex, on the average filament length at steady state. We developed two mechanisms of the side branching: the Arp2/3 complex random nucleation to only ATF or to either ATF/APF/ADF. The latter case, despite not yielding a difference between nSRF and SRF models even at steady state, is needed to validate the simulation algorithms (Fig. 4F, inset). The average filament length in the steady-state phase decreases with the concentration of the Arp2/3 complex by both nSRF and SRF models – as is indeed expected from previous analytical calculations [47]. In **Supplementary material** we show an additional simulation example demonstrating that the outcome of Arp2/3 –complex association and side branch initiation, which preferably occurs at an ATP-charged protomer, may differ for SRF and nSRF models (see Fig. S3).

Based on the synthetic data we obtained for systems with increasing complexity and from comparing the two models where one model ignores the positional information of actin monomers in the filament, one is lead to conclude that unless the system is deprived of ATP-actin, both models yield the same result. This surprisingly suggests that the relative positions of ATP-actin and ADP-actin protomers within a filament are not important. One possible explanation is that the ATP hydrolysis rate does not influence the early time kinetics because it is very slow (0.0007 s^{-1}). This

interpretation explains why kinetic models without ATP hydrolysis are also successful. Once the system reaches the steady state phase, however, the nucleotide status may play a significant role for actin polymerisation (as demonstrated in Fig 4B) for severing of filaments by cofilin (at ADP-actin protomers) or branching by Arp2/3 complex (at ATP-actin protomers as shown in Fig S3, **Supplementary material**). In this case the developed SRF will yield more accurate results.

Additional numerical tests on validation of the developed models, in particular, effects of capping protein concentration and of various rate constants on actin polymerization, are reported in **Supplementary material**. Collectively, this leads to the following conclusions. Increasing the concentration of capping proteins leads to increase of the overall polymerization rate due to faster nucleation. Interestingly, if we exclude the nucleation activity of capping proteins, pointed-end capping proteins had no significant effect on actin polymerization kinetics. Second, we detected that already a moderate, twofold increase/decrease in monomer association/dissociation rates at the barbed ends strongly affects actin polymerization kinetics and almost no effect can be seen for the pointed ends. The simulation shows that increasing the nucleation rate results in a considerable rise in polymerized actin. Finally, variation in the aging rate does not modify the actin polymerization kinetics until steady-state is reached.

4.4. Evaluation on experimental data

To further evaluate the robustness of the developed models, we applied them to fitting of experimental data.

4.4.1. Actin polymerization

The simulation for 2 and 3 μM of actin concentrations has been performed with the same nucleation rate k_{SNUC} = 4.1x10^{-9} μM^{-2}s^{-1}. The results of the comparison are given in Fig. 5A. Possible inconsistency between simulated and experimental data would result in curvature difference. Simulated and experimental data were however in good agreement, although small non-significant differences could be observed (3 μM of actin, top curve).

4.4.2. Actin polymerization in the presence of capping proteins

We next evaluated the effect of barbed end capping protein. We tested our models on data published previously in [14]. Keeping the actin concentration constant (2 μM), the concentration of CBM was increased between 0 and 25 nM. The resulting change in pyrene fluorescence in time is given by solid lines in Fig. 5B. These experimental data and the simulation results, presented by symbols, highly correlated. The best fitting was obtained with the nucleation rate k_{CBNU} = 1.2x10^{-5} μM^{-3}s^{-1} only slightly differed from the 10^{-5} μM^{-3}s^{-1} used in numerical tests of sections 4.2.2. − 4.3.2.

4.4.3. Formin-actin polymerization

The experimental assay included 6 μM actin and 0.2 μM formin (in the absence of profilin). First, we fixed the formin-enhanced elongation rate of actin filament, taking the value of k_{FASB} = 9 μM^{-1}s^{-1} [12]. Then the nucleation rate was fitted. The best fit (Fig. 5C) was obtained for a nucleation rate constant of k_{FNUC} = 4.7x10^{-7}μM^{-3}s^{-1}, which is ~10 times higher than the value for spontaneous actin nucleation. We could get acceptable fittings with other combinations of values for k_{FASB} and k_{FNUC}, for example, with k_{FASB} = 90 μM^{-1}s^{-1} and k_{FNUC} = 4.7x10^{-8} μM^{-3}s^{-1}, indicating that the elongation rate and nucleation rate are highly correlated.

4.5. Software ActinSimChem

Although numerous software packages are available for biochemical kinetic modelling, no dedicated, Windows-based software which meets all the needs arising from analysis of any specific actin polymerization system is currently available. Therefore a new stand-alone software package, *ActSimChem*, for the here presented Monte Carlo simulation of actin polymerization processes has been developed (for details see **Supplementary material**). *ActSimChem* provides the possibility for: i) switching between the nSRF and SRF models; ii) input/variation of the model parameters; iii) a compact set of the stochastic modelling algorithms (including the developed modifications of the Gillespie's "direct", the “first reaction”, the "next reaction" methods); iv) simulation of actin

polymerization (currently up to 21 molecular and 28 chemical actin-related reactions); v) graphical representation of simulation results; vi) storage of the results. The program and its manual can be obtained on request or can be downloaded from the website http://actinsim.uni.lu.

5. Concluding remarks

We have developed and compared two stochastic simulation models of actin polymerization processes connecting multiple main actin polymerization-related biochemical reactions including spontaneous and enhanced actin nucleation, association/dissociation at filaments barbed and pointed ends, filament branching, fragmentation and annealing. Additionally the action of different actin-accessory protein that regulate filament dynamics, the structural composition of filaments and the distribution of filament lengths can be simulated. We evaluated the computational efficiency and simulation accuracy of the nSRF and SRF models, that differ in presentation of structural, i.e. ATP-hydrolysis-related, properties of actin filaments. In the majority of numerical tests, the nSRF model considerably saved computational time and still gave outcome characteristics at the same confidence level as the complete SRF model. This result realistically enables the nSRF model to be applied for experimental data fitting and for deriving reaction rate constants on the same manner as reported in [48-50]. For situations were ATP-actin monomers are limiting the SRF model needs, however, to be used.

The presented stochastic methodology forms a considerable improvement upon recently reported models [23, 24] in at least four ways. First, the number of already incorporated actin-polymerization reactions is very high. This allows evaluating outcome of complex biosystems closer to physiological situations, thus adding predictive power. Second, the Monte Carlo-based simulation algorithms are efficient and robust. Third, the open-architecture principle in the integrated modelling of actin-associated reactions events and filaments structures ensures flexibility in combination with a broad applicability. This architecture allows upgrading the utilised stochastic simulation algorithm for any newly-developed advanced modelling technique on the one hand, and permits further extension of the simulated system for additional actin-interacting proteins and

polymerization mechanisms on the other hand. Fourth, we provide a free and user-friendly software package *ActinSimChem*, that contains the developed simulation algorithms. The package can be used to simulate *in silico* the numerical time-resolved outcome under form of the actin filament concentration and distribution of filament lengths for a complex set of actin-polymerization processes. This unique tool for simulation or fitting experimental data, will allow biologists comparing existing actin-polymerization systems and more easily design and interpret complex experiments in which more than "reaction" on actin is taking place.

As demonstrated potential of our model, we performed in this article several numerical experiments on simulations of known and well-established actin polymerization systems. The results of these computer tests underscored important aspects of actin dynamics, namely that: i) under the conditions used, the reactions at pointed ends and by pointed-end capping proteins do not exhibit a significant effect on actin polymerization, unless pointed-end capping proteins work as nucleators; ii) the aging reaction has a minor effect on early state actin polymerization kinetics and only has an effect when equilibrium is reached; iii) nucleation and elongation are correlated when considering time evolution of actin in the filamentous form.

ACKNOWLEDGMENTS

This work was supported by *Fonds National de la Recherche*, Luxembourg (grant nr FNR/05/MA6/17), Human Frontier Science Program (grant nr RGP0058/2005) and the FWO-Vlaanderen to MVT and CA (grant nr G.0157.05), CNRS. AAH was a recipient of an ESF Exchange Visit Grant.

Appendix A. Supplementary material

Supplementary material associated with this article contains: evaluation of the biochemical parameters, validation of the source code, comparison of the stochastic simulation algorithms, methodology of error analysis, the rate equations for an actin system and an actin and capping protein system, summary on the software package *ActinSimChem*, and additional simulation data

References

[1] A. Giganti, J. Plastino, B. Janji, M. Van Troys, D. Lentz, C. Ampe, C. Sykes, E. Friederich, Actin-filament cross-linking protein T-plastin increases Arp2/3-mediated actin-based movement, J. Cell Sci. 118 (2005) 1255-1265.

[2] A. Lambrechts, M. Van Troys, C. Ampe, The actin cytoskeleton in normal and pathological cell motility, The international journal of biochemistry & cell biology 36 (2004) 1890-1909.

[3] C. Le Clainche, M.F. Carlier, Regulation of actin assembly associated with protrusion and adhesion in cell migration, Physiological reviews 88 (2008) 489-513.

[4] M. Van Troys, L. Huyck, S. Leyman, S. Dhaese, J. Vandekerkhove, C. Ampe, Ins and outs of ADF/cofilin activity and regulation, European journal of cell biology (2008).

[5] D. Yamazaki, S. Kurisu, T. Takenawa, Regulation of cancer cell motility through actin reorganization, Cancer Sci. 96 (2005) 379-386.

[6] A. Giganti, E. Friederich, The actin cytoskeleton as a therapeutic target: state of the art and future directions, Prog. Cell Cycle Res. 5 (2003) 511-525.

[7] F.S. Soo, J.A. Theriot, Large-scale quantitative analysis of sources of variation in the actin polymerization-based movement of Listeria monocytogenes, Biophys. J. 89 (2005) 703-723.

[8] A. Lambrechts, K. Gevaert, P. Cossart, J. Vandekerckhove, M. Van Troys, Listeria comet tails: the actin-based motility machinery at work, Trends in cell biology 18 (2008) 220-227.

[9] T.D. Pollard, G.G. Borisy, Cellular motility driven by assembly and disassembly of actin filaments, Cell 112 (2003) 453-465.

[10] A. Mogilner, Mathematics of cell motility: have we got its number?, Journal of mathematical biology (2008).

[11] S. Romero, C. Le Clainche, D. Didry, C. Egile, D. Pantaloni, M.F. Carlier, Formin is a processive motor that requires profilin to accelerate actin assembly and associated ATP hydrolysis, Cell 119 (2004) 419-429.

[12] D.R. Kovar, Molecular details of formin-mediated actin assembly, Curr. Opin. Cell Biol. 18 (2006) 11-17.

[13] M. Pring, M. Evangelista, C. Boone, C. Yang, S.H. Zigmond, Mechanism of formin-induced nucleation of actin filaments, Biochemistry 42 (2003) 486-496.

[14] A.E. Carlsson, M.A. Wear, J.A. Cooper, End versus side branching by Arp2/3 complex, Biophysical journal 86 (2004) 1074-1081.

[15] T.D. Pollard, C.C. Beltzner, Structure and function of the Arp2/3 complex, Curr. Opin. Struct. Biol. 12 (2002) 768-774.

[16] R.E. Mahaffy, T.D. Pollard, Kinetics of the formation and dissociation of actin filament branches mediated by Arp2/3 complex, Biophys. J. 91 (2006) 3519-3528.

[17] J.A. Cooper, T.D. Pollard, Effect of capping protein on the kinetics of actin polymerization, Biochemistry 24 (1985) 793-799.

[18] A. Matzavinos, H.G. Othmer, A stochastic analysis of actin polymerization in the presence of twinfilin and gesolin, J. Theor. Biol. (2007).

[19] V. DesMarais, M. Ghosh, R. Eddy, J. Condeelis, Cofilin takes the lead, J. Cell Sci. 118 (2005) 19-26.

[20] A.E. Carlsson, Stimulation of actin polymerization by filament severing, Biophys. J. 90 (2006) 413-422.

[21] J.L. McGrath, E.A. Osborn, Y.S. Tardy, C.F. Dewey, Jr., J.H. Hartwig, Regulation of the actin cycle in vivo by actin filament severing, Proc. Natl. Acad. Sci. USA 97 (2000) 6532-6537.

[22] K. Binder, M.H. Kalos, Monte Carlo methods in statistical physics, Springer, Berlin, 1979.

[23] F.J. Brooks, A.E. Carlsson, Actin polymerization overshoots and ATP hydrolysis as assayed by pyrene fluorescence, Biophysical journal 95 (2008) 1050-1062.

[24] J. Roland, J. Berro, A. Michelot, L. Blanchoin, J.L. Martiel, Stochastic severing of actin filaments by actin depolymerizing factor/cofilin controls the emergence of a steady dynamical regime, Biophysical journal 94 (2008) 2082-2094.

[25] J. Fass, C. Pak, J. Bamburg, A. Mogilner, Stochastic simulation of actin dynamics reveals the role of annealing and fragmentation, Journal of theoretical biology 252 (2008) 173-183.

[26] M.M. Yatskou, H. Donker, E.G. Novikov, R.B.M. Koehorst, A. van Hoek, V.V. Apanasovich, T.J. Schaafsma, Nonisotropic excitation energy transport in organized molecular systems: Monte Carlo simulation-based analysis of time-resolved fluorescence, J. Phys. Chem. A 105 (2001) 9498-9508.

[27] P.V. Nazarov, V.V. Apanasovich, V.M. Lutkovski, M.M. Yatskou, R.B. Koehorst, M.A. Hemminga, Artificial neural network modification of simulation-based fitting: application to a protein-lipid system, J. Chem. Inf. Comput. Sci. 44 (2004) 568-574.

[28] A.F. Maree, A. Jilkine, A. Dawes, V.A. Grieneisen, L. Edelstein-Keshet, Polarization and movement of keratocytes: a multiscale modelling approach, Bull Math Biol 68 (2006) 1169-1211.

[29] C. Neidl, J. Engel, Exchange of ADP, ATP and 1: N6-ethenoadenosine 5'-triphosphate at G-actin. Equilibrium and kinetics, Eur J Biochem 101 (1979) 163-169.

[30] J.L. McGrath, Y. Tardy, C.F. Dewey, Jr., J.J. Meister, J.H. Hartwig, Simultaneous measurements of actin filament turnover, filament fraction, and monomer diffusion in endothelial cells, Biophysical journal 75 (1998) 2070-2078.

[31] J. Lippincott-Schwartz, E. Snapp, A. Kenworthy, Studying proteins dynamics in living cells, Nat. Cell Biol. Rev. 2 (2001) 444–456.

[32] B.L. Sprague, R.L. Pego, D.A. Stavreva, J.G. McNally, Analysis of binding reactions by fluorescence recovery after photobleaching, Biophysical journal 86 (2004) 3473-3495.

[33] K. Braeckmans, K. Remaut, R.E. Vandenbroucke, B. Lucas, S.C. De Smedt, J. Demeester, Line FRAP with the confocal laser scanning microscope for diffusion measurements in small regions of 3-D samples, Biophysical journal 92 (2007) 2172-2183.

[34] D.T. Gillespie, A general method for numerically simulating the stochastic time evolution of coupled chemical reactions, J. Comput. Phys. 22 (1976) 403-434.

[35] M.A. Gibson, J. Bruck, Efficient exact stochastic simulation of chemical systems with many species and many channels, J. Phys. Chem. A 104 (2000) 1876-1889.

[36] D.T. Gillespie, Approximate accelerated stochastic simulation of chemically reacting systems, J. Chem. Phys. 115 (2001) 1716-1733.

[37] D.T. Gillespie, Exact stochastic simulation of coupled chemical reactions, J. Phys. Chem. 81 (1977) 2340-2361.

[38] S.K. Maciver, A.G. Weeds, Actophorin preferentially binds monomeric ADP-actin over ATP-bound actin: consequences for cell locomotion, FEBS Lett 347 (1994) 251-256.

[39] J.A. Spudich, S. Watt, The regulation of rabbit skeletal muscle contraction. I. Biochemical studies of the interaction of the tropomyosin-troponin complex with actin and the proteolytic fragments of myosin, The Journal of biological chemistry 246 (1971) 4866-4871.

[40] T. Kouyama, K. Mihashi, Fluorimetry study of N-(1-pyrenyl)iodoacetamide-labelled F-actin. Local structural change of actin protomer both on polymerization and on binding of heavy meromyosin, Eur J Biochem 114 (1981) 33-38.

[41] M.F. Carlier, D. Pantaloni, E.D. Korn, Evidence for an ATP cap at the ends of actin filaments and its regulation of the F-actin steady state, The Journal of biological chemistry 259 (1984) 9983-9986.

[42] L. Blanchoin, T.D. Pollard, Hydrolysis of ATP by polymerized actin depends on the bound divalent cation but not profilin, Biochemistry 41 (2002) 597-602.

[43] M. Bindschadler, E.A. Osborn, C.F. Dewey, Jr., J.L. McGrath, A mechanistic model of the actin cycle, Biophysical journal 86 (2004) 2720-2739.

[44] D. Vavylonis, Q. Yang, B. O'Shaughnessy, Actin polymerization kinetics, cap structure, and fluctuations, Proc Natl Acad Sci U S A 102 (2005) 8543-8548.

[45] L.S. Tobacman, E.D. Korn, The kinetics of actin nucleation and polymerization, The Journal of biological chemistry 258 (1983) 3207-3214.

[46] D. Sept, J. Xu, T.D. Pollard, J.A. McCammon, Annealing accounts for the length of actin filaments formed by spontaneous polymerization, Biophysical journal 77 (1999) 2911-2919.

[47] A.E. Carlsson, The effect of branching on the critical concentration and average filament length of actin, Biophysical journal 89 (2005) 130-140.

[48] M.M. Yatskou, M. Meyer, S. Huber, M. Pfenniger, G. Calzaferri, Electronic excitation energy migration in a photonic dye--zeolite antenna, Chemphyschem 4 (2003) 567-587.

[49] P.V. Nazarov, R.B. Koehorst, W.L. Vos, V.V. Apanasovich, M.A. Hemminga, FRET study of membrane proteins: simulation-based fitting for analysis of membrane protein embedment and association, Biophys. J. 91 (2006) 454-466.

[50] D. Marushchak, S. Grenklo, T. Johansson, R. Karlsson, L.B. Johansson, Fluorescence Depolarisation Studies of Filamentous Actin Analysed with a Genetic Algorithm, Biophysical journal (2007).

[51] S. Samarin, S. Romero, C. Kocks, D. Didry, D. Pantaloni, M.F. Carlier, How VASP enhances actin-based motility, J. Cell Biol. 163 (2003) 131-142.

[52] D. Sept, J.A. McCammon, Thermodynamics and kinetics of actin filament nucleation, Biophys. J. 81 (2001) 667-674.

[53] T.D. Pollard, Rate constants for the reactions of ATP- and ADP-actin with the ends of actin filaments, J. Cell Biol. 103 (1986) 2747-2754.

[54] D. Schafer, P. Jennings, J. Cooper, Dynamics of capping protein and actin assembly in vitro: Uncapping barbed ends by polyphosphoinisitides, J. Cell Biol. 135 (1996) 169-179.

[55] J.R. Kuhn, T.D. Pollard, Real-time measurements of actin filament polymerization by total internal reflection fluorescence microscopy, Biophysical journal 88 (2005) 1387-1402.

[56] A. Mogilner, L. Edelstein-Keshet, Regulation of actin dynamics in rapidly moving cells: a quantitative analysis, Biophys. J. 83 (2002) 1237-1258.

TABLES

Table 1. Simulated reactions and corresponding rate constants (for abbreviations of reagents see the section Abbreviations used).

Reaction and equation	**Symbol**	**Values [ref.]**
Spontaneous nucleation of the filament 3 ATM $\rightarrow$ 3 ATF + FTB + FTP *	k_{SNUC}	$2.3x10^{-11}$ $\mu M^{-2}s^{-1}$ [51]; $1.1x10^{-9}$ $\mu M^{-2}s^{-1}$ [14]; ~ $2x10^{-8}$ $\mu M^{-2}s^{-1}$ [52]
Formin-initiated nucleation FOM + 3 ATM $\rightarrow$ 3 ADF + FOF + FDP	k_{FNUC}	$7x10^{-5}$ $\mu M^{-3}s^{-1}$ [13]
Nucleation by barbed-end capping protein CBM + 3 ATM $\rightarrow$ 3 ATF + CBF + FTP	k_{CBNU}	used in simulations – 10^{-5} $\mu M^{-3}s^{-1}$; for six ATM – $2.94x10^{-5}$ $\mu M^{-6}s^{-1}$ [14]
Nucleation by pointed-end capping protein CPM + 3 ATM $\rightarrow$ 3 ATF + CPF + FTB	k_{CPNU}	no data
ATP-actin association at barbed end FxB** + ATM $\rightarrow$ FTB + ATF	k_{ASTB}	11.5 $\mu M^{-1}s^{-1}$ [53]
ADP-actin association at barbed end FxB + ADM $\rightarrow$ FDB + ADF	k_{ASDB}	3.8 $\mu M^{-1}s^{-1}$ [53]
ATP-actin association at pointed end FxP + ATM $\rightarrow$ FTP + ATF	k_{ASTP}	1.3 $\mu M^{-1}s^{-1}$ [53]
ADP-actin association at pointed end FxP + ADM $\rightarrow$ FDP + ADF	k_{ASDP}	0.16 $\mu M^{-1}s^{-1}$ [53]
Dissociation of ATP-actin from barbed end FTB $\rightarrow$ FxB + ATM(+FRP)	k_{DITB}	1.4 s^{-1} [53]
Dissociation of ADP-Pi-actin from barbed end FPB $\rightarrow$ FxB + ADM(+FRP)	k_{DIPB}	1.4 s^{-1} [25, 53]

Dissociation of ADP-actin from barbed end	k_{DIDB}	7.2 s^{-1} [53]
FDB → FxB + ADM(+FRP)		
Dissociation of ATP-actin from pointed end	k_{DITP}	0.8 s^{-1} [53]
FDB → FxB + ATM(+FRP)		
Dissociation of ADP-Pi-actin from pointed end	k_{DIPP}	0.8 s^{-1} [25, 53]
FPP → FxP + ADM(+FRP)		
Dissociation of ADP-actin from pointed end	k_{DIDP}	0.27 s^{-1} [53]
FDB → FxB + ADM(+FRP)		
Capping of the barbed end	k_{ASCB}	3.0 $\mu M^{-1}s^{-1}$ [54]
CBM + FxB → CBF		8.0 $\mu M^{-1}s^{-1}$ [14]
Capping of the pointed end	k_{ASCP}	~ 0.25 – 1.0 $\mu M^{-1}s^{-1}$ [14]
CPM + FxP → CPF		
Uncapping of the barbed end	k_{DICB}	4.0x10^{-4} s^{-1} [54]
CBF → CBM + FxB		4.2 s^{-1} [14]
Uncapping of the pointed end	k_{DICP}	no data
CPF → CPM + FxP		
Association of formin to barbed end	k_{ASFB}	no data
FOM + FxB → FOF		
Detachment of formin from barbed end	k_{DIFB}	7.5 x 10^{-4} s^{-1} [11]
FOF → FOM + FDB		
Formin-initiated association at barbed end	k_{FASB}	for mDia formin in the presence of
FOF + ATM → FOF + ADF		profilin 45-110 $\mu M^{-1}s^{-1}$ [11, 12]
		without profilin – 9 $\mu M^{-1}s^{-1}$ [12]
Arp2/3 association to the F-actin	k_{ASRT}	5.4 x 10^{-4} $\mu M^{-3}s^{-1}$ [14]
AxF+ARM → AxF+ARF+FRB		

Dissociation of the Arp 2/3 from the pointed end FRP[+ARF] → ARM+FxP	k_{DIRP}	0.0018 s^{-1} [14]
Fragmentation: ^ → FyB+FxP	k_{FRGM}	no data
Annealing: FyB+FxP →^	k_{ANNL}	no data
ATP-hydrolysis: ATF → APF	k_{TTOP}	0.3 s^{-1} [42, 55]
Phosphate release: APF → ADF	k_{PTOD}	0.0026 s^{-1} [43, 55]
Recharge of monomeric actins in the pool ADM → ATM	k_{DTOT}	~20 (pro) s^{-1} [56]

* An experimental and theoretical study, reported in [52], indicates that the trimer is the critical nucleus for spontaneous nucleation of actin monomers. The spontaneous actin nucleation can be well approximated by a third order nucleation step for an actin monomer concentration higher or equal to 2 μM [14]]. Other hypotheses on mechanism of spontaneous filament nucleation, including explicit, coupled nucleation steps may be implemented within the frame of our simulation scheme.

** FxB stands for the types of barbed ends: FTB, FPB, FDB and FRB; FyB for FTB, FPB, FDB; FxP for FTP, FPP and FDP and AxF for ATf, APF and ADF; ^ denotes the position between two actin protomers in filament.

Captions for figures

Fig. 1. Diagrams of simulated actin-polymerization processes (for the non-mentioned rate constants see Table 1, for abbreviations of reagents see the section Abbreviations used).

Fig. 2. Integrative stochastic simulation model of actin polymerization processes. (A) Schematic diagram of the developed simulation model. Presently, we incorporated n_R = 21 molecular reagents participating in M = 28 chemical actin-related reactions (*cf.* Table 1). SSS – stochastic simulation scheme. (B) Flow diagram for the stochastic simulation scheme. Vector $\mathbf{N} = \{N_k\} = (N_{ATM}, N_{ADM}, \ldots, N_{FRB})$ contains the number of molecules of each reagent. The evolution vector **N** in time is denoted as $\mathbf{N}(t)$.

Fig. 3. Predicted concentrations of F-actin by the nSRF (symbols) and analytical models (lines) for (A) actin polymerisation and (B) actin polymerisation in presence of a filament barbed end capping protein, (A) $[ATM]_{t=0}$ = 3, 6 and 12 μM (bottom, middle and top curves), $k_{SNUC} = 10^{-8}$ $\mu M^{-2}s^{-1}$, (B) $[ATM]_{t=0}$ = 2 μM, $[CBM]_{t=0}$ = 0.1 μM (top curve) and 0.01 μM (bottom curve), $k_{CBNU} = 10^{-5}$ $\mu M^{-3}s^{-1}$. If a parameter is not mentioned specifically, the value from Table 1 is used.

Fig. 4. Predicted concentrations of F-actin by the SRF (symbols) and nSRF (lines) models in function of time.

(A) Actin polymerisation, $[ATM]_{t=0}$ = 3, 6 and 9 μM (bottom, middle and top curves in the plot), $k_{SNUC}=10^{-8}$ $\mu M^{-2}s^{-1}$.

(B) Actin polymerisation without monomer recharge (k_{DTOT} = 0 s^{-1}), simulated for a long time period, $[ATM]_{t=0}$ = 2 μM, $k_{SNUC} = 10^{-6}$ $\mu M^{-2}s^{-1}$ and $k_{TTOD} = 10^{-2}$ s^{-1}.

(C) Actin polymerisation in presence of a filament barbed end capping protein, $[ATM]_{t=0}$ =3 μM, $[CBM]_{t=0}$ = 0.1 μM (top curve) and $[CBM]_{t=0}$ = 0.01 μM (bottom curve), $k_{CBNU} = 10^{-5}$ $\mu M^{-3}s^{-1}$.

(D) Actin polymerisation in presence of a filament pointed end capping protein, $[ATM]_{t=0}$ = 3 μM; $[CPM]_{t=0}$ = 0.1 μM (top curve) and $[CPM]_{t=0}$ = 0.01 μM (bottom curve), $k_{CPNU} = 10^{-5}$ $\mu M^{-3}s^{-1}$.

(E) Formin-initiated actin polymerization, the top curve corresponds to 0.1 μM of formin, the bottom curve to 0.01 μM; $k_{FNUC} = 7x10^{-5}$ $\mu M^{-3}s^{-1}$, $k_{FASB} = 110$ $\mu M^{-1}s^{-1}$.

(F) Actin polymerisation in the presence of all reagents (ATM, CBM, CPM, FOM, ARM) included and branching to either ATF/APF/ADF. The top curve corresponds to 3 μM of actin, the bottom curve to 2μM. (*Inset*) Decrease of the average filament length <*L*> in the steady-state phase with the concentration of the Arp2/3 complex (2 μM of actin). $[CBM]_{t=0}$=$[CPM]_{t=0}$=0.01 μM, $[FOM]_{t=0}$=0.001 μM, $[ARM]_{t=0}$=0.01 μM, $k_{SNUC} = 10^{-8}$ $\mu M^{-2}s^{-1}$, $k_{CBNU} = k_{CPNU} = 10^{-5}$ $\mu M^{-3}s^{-1}$, $k_{FNUC} = 7x10^{-5}$ $\mu M^{-3}s^{-1}$, $k_{FASB} = 110$ $\mu M^{-1}s^{-1}$, $k_{FRGM} = 1.8\times10^{-8}$ s^{-1}, $k_{ANNL} = 10^{-8}$ $\mu M^{-1}s^{-1}$, $k_{ASRT} = 10^{-5}$ $\mu M^{-1}s^{-1}$, $k_{DIRP} = 10^{-3}$ s^{-1}. If a parameter is not mentioned specifically, the value from Table 1 is used.

Fig. 5. Comparison of the simulation results (symbols) with experimentally obtained data (solid lines).

(A) Actin assay with $[ATM]_{t=0}$ = 2 μM (bottom curve) and 3 μM (top curve). Experimental fluorescence data were corrected for background and normalized by amplitude to fit simulated concentrations. During simulation $k_{SNUC} = 4.1x10^{-9}$ $\mu M^{-2}s^{-1}$, the other rates are the same as listed in Table 1.

(B) Experimental data showing the effect of capping-protein nucleation from [14] (solid lines). Experimental assays contain 2 μM of actin and various concentrations of barbed-end capping protein: $[CBM]_{t=0}$ = 0, 5, 15 and 25 nM.

(C) Formin-initiated actin polymerization. Here the comparison of the experimental fluorescence data (solid line), normalized by amplitude, and simulation results for two models of formin-actin polymerization (symbols) are given. The experimental sample contains $[ATM]_{t=0}$ = 6 μM and $[FOM]_{t=0}$ = 0.2 μM. Black triangles corresponds to the model with $k_{FASB} = 9$ $\mu M^{-1}s^{-1}$ and $k_{FNUC} = 4.7x10^{-7}\mu M^{-3}s^{-1}$. White circles corresponds to the model with $k_{FASB} = 90$ $\mu M^{-1}s^{-1}$ and $k_{FNUC} = 4.7x10^{-8}\mu M^{-3}s^{-1}$.

Supplementary material

to the manuscript:

An Integrative Stochastic Simulation Model Linking Major Biochemical Reactions of Actin-Polymerization to Structural Properties of Actin Filaments

Aliaksandr A. Halavatyi, Petr V. Nazarov, Sandrine Medves, Marleen van Troys, Christophe Ampe, Mikalai Yatskou, Evelyne Friederich

Evaluation of the biochemical parameters

To investigate further the consistency of systems behaviour, we tested the effects of variations of biochemical parameters on the simulation results.

Sensitivity to concentrations

We first evaluated the influence of concentration effects. The concentration of actin monomers affects two key steps of the polymerization kinetics (see Fig. 4 A, Manuscript): the rate of spontaneous nucleation, which is, at least in a cubic, proportional to actin monomer concentration (Table 1, Manuscript) and the elongation rate. Capping proteins work as a filament nucleator and cap the corresponding ends of filaments, stopping both elongation and dissociation at that end. Both effects are depicted in Fig. S4 A (barbed-end capping protein) and S4 B (pointed end capping proteins). Obviously, increasing the concentration of these proteins leads to increase of the overall polymerization rate due to faster nucleation. Even for barbed-end capping proteins this holds true, however, the effect is less pronounced then in the case of pointed-end cappers, because the filaments exclusively elongate from their minus end. As a consequence, the critical concentration (steady-state concentration of actin monomers) is higher in the presence of barbed-end capping proteins.

If we exclude the nucleation activity of capping proteins, i.e. setting k_{CBNU}=k_{CPNU} = 0, the concentration dependency significantly changes. As expected from experimental data, the increase of barbed-end capping protein concentration leads now to a decrease of the polymerization rate (Fig. S4 C). A saturation effect can be observed in this plot since almost no difference in actin dynamics can be seen using a concentration of capping proteins of 0.1 to 1 μM. This corresponds to the situation when all barbed ends are capped.

Interestingly, pointed-end capping proteins had no significant effect on actin polymerization kinetics (Fig. S4 D). Concentration variation of the pointed-end capping protein by a factor of 1000, ranging from 0.001 to 1 μM, did not affect actin polymerization kinetics under the assumption that the capping protein does not act as a nucleator.

Among the proteins we considered, formin had the most pronounced effect. It works both as a nucleator and an enhancer of the elongation [1] and this is evident from Figures 4E and 5C, Manuscript. Due to its high nucleation ability, almost no *lag phase* is observed in the simulations and in the pyrene-actin experiments for formin-containing samples.

Sensitivity to the rate constants

We estimated the effects of various rate constants on actin polymerization. The association and dissociation rate constants of ATP-actin monomers to or from actin filaments were first investigated (Fig. S4 E and F). Fig. S4 E shows that already a moderate, two fold increase (top curve, squares) or decrease (bottom curve, triangles) in monomer association and dissociation rates at the barbed ends strongly affects actin polymerization kinetics. However, if the same numerical experiment is performed for the pointed ends, almost no effect can be seen (Fig. S4 F). This is due to the fact that the actin exchange at the pointed ends is approximately 10 times slower than that at the barbed ends and thus elongation proceeds mainly via the

barbed end. This underscores why in cells the actin system requires a more extensive array of barbed end regulators.

Fig. S4 G shows the effect of the spontaneous nucleation (the rate k_{SNUC}) on actin polymerization. The change in k_{SNUC} from 10^{-9} to $5x10^{-9}$ $\mu M^{-2}s^{-1}$ leads to significant changes in the predicted concentration of F-actin protomers (diamonds and triangles in Fig. S4 G). The simulation shows that increasing the nucleation rate results in a considerable increase in polymerized actin due to the formation of oligomeric nuclei. It suggests that the spontaneous nucleation is an important effect that plays a key role in polymerization and thus cannot be neglected or shut off during analysis of experimental systems with computational models. However, our simulations do not provide the exact value of the elongation rate constant at which nuclei started to grow since the elongation process may generally be depended on other systems parameters, such as association/dissociation rates of monomers at plus ends, that often might hardly be distinguishable in experiments.

Fig. S4 H demonstrates the effect of filament aging on the concentration of F-actin. Variation in the aging rate does not modify the actin polymerization kinetics until steady-state is reached. Moreover, changing of k_{TTOD} from $7x10^{-4}$ s^{-1} to 0.7 s^{-1} has only a minor effect on the steady state level of protomer concentration. This is not surprising since polymerization of pure actin is uncoupled from ATP hydrolysis.

Validation of the source code

To ensure the quality of the simulation algorithm we performed several validation procedures. Our simulation algorithms were tested against reported analytical models covering some selected idealised actin systems of a relatively limited number of reagents and reactions. Any further update of the simulation model, by adding additional reagents or reactions, does/will not perturb the stochastic simulation scheme since the procedure of decision control at each simulation step is integrative and hierarchically built in terms of reagents and reactions. The extension of the model with new reagents and reactions consists in updating classes of individual filaments and properties of simulated volume. In order to control a balance between internal/external objects of the classes and limits for systems parameters we developed a dedicated debug system. The debug procedure summarizes any quantities of objects of check-in properties and compares the matching with numbers of currently simulated molecules for the considered reagents, e.g. – a number of filament branches with capped barbed ends or a number of the ATF protomers. For SRF model an additional validation step was implemented that verifies the nucleotide sequence of filament subunits.

In order to extensively validate the source code, the debug procedure was launched after simulation of each reaction shown in Fig. 1, Manuscript. The code was verified for a wide range of reaction rate constants, typically covering ±2 orders of magnitudes from the values presented in Table 1, Manuscript, and validated for simulated volumes higher than 30 μm^3.

Comparison of the simulation algorithms

We examined several formulations of the main stochastic simulation algorithm. In particular, the exact Gillespie's "direct" and "first reaction" and the "next reaction" algorithms [2]. The inexact "τ-leap" algorithm has been tested as well.

The "next reaction" algorithm is the improvement of the "direct" and "first reaction" algorithms, where three specific features are implemented: i) in each modelling iteration just one random number is generated (*versus* two random numbers in the "direct" method and *l* random numbers in "first reaction" algorithm, where *l* is the number of reactions in a system); ii) an advanced search of a minimal value for the reaction time due to indexed priority queue; iii) re-calculation of reaction probabilities a_i, (*cf.* Eq. (1), (2), Manuscript) for those reactions that were affected in the current simulation cycle; subsequently, the dependency graph is constructed. In this graph, nodes represent the reactions in the system, an edge from the *i*-th node to *j*-th node is drawn if the *i*-th reaction influences the probability a_j of *j*-th reaction. For our models the *a priori* prediction of this graph is not evident, because many reactions have multiple outcome and can potentially change different concentrations, e.g. the dissociation of an ATF monomer from a barbed end can result in

changing either two concentrations, [ATF] and [ATM], or four concentrations, [ATF], [ATM], [FTB], [FDB], or even more concentrations in the case of complete filament dissociation. Therefore in our realization of the Gibson-Bruck algorithm, we introduced only the repeatable usage of the random events times and advanced search of minimal time.

The comparison of the algorithms was performed for several compositions of the actin system: actin alone, actin with barbed-end capping protein, actin with pointed-end capping protein, actin with capping proteins of both types, actin with formin, and finally the mix of all mentioned reagents, except the Arp2/3 complex. The initial concentrations of reagents were: $[ATM]_{t=0}$ = 2 μM, $[CBM]_{t=0}$ = $[CPM]_{t=0}$ = 10^{-2} μM, $[FOM]_{t=0}$ = 10^{-3} μM. The maximal simulation time t_{max} was 8000 s. Computer simulations were performed for a volume V equal to 8000 μm^3. The resulted times spent for the simulations by the "direct" and "first reaction", "next reaction" algorithms are plotted in Fig. S5 A. The Gillespie's "direct" modelling technique has demonstrated the most efficient in time simulations.

The “first’ reaction method was found as the slowest one among the modelling methods. It is due to enormous generation of random numbers in modelling of one reaction. The modelling by the “next reaction” algorithm was faster than “first reaction” method, but obviously slower than the Gillespie's direct algorithm. A similar observation for these three methods has been reported in [3]. According to the conclusions made by Cao et al, the “direct” algorithm works faster than the “next reaction” algorithm when the occurrence of a reaction influences probability values a_i for a small number of reactions, i.e. each node of the directed graph has a few incoming and outgoing edges. In our case, when the current reaction may have an influence on many reaction probabilities a_i, the realization of a dependency graph would not give any improvement for simulation speed, even if it was algorithmically realistic.

The inexact "τ-leap" algorithm was found unusable for the systems under consideration here. It simulates properly the molecular systems where the number of molecules in a molecular pool significantly exceeds the number of reacting molecules during each time step. This is not the case in our modelled systems where the filament binding sites are approaching the low concentration of 10^{-10} M.

Error analysis

The analysis of the approximation error of the simulation model is an important factor to take into account when evaluating results of computer simulations. One of the chief concerns is to be able to get as accurate an approximation as possible. Increasing the simulated volume V or/and averaging the results of n_A independent simulations may improve the approximation accuracy in simulations. We therefore discuss here the associated error statistics and computational efficiency of the developed models.

As an approximation error we chose the sum of squared residuals E of the simulated data S and the precise or reference data F. Such reference data are expected to be either an exact solution or a stochastic approximation at $n_A \to \infty$ and $V \to \infty$. Then, the equation for E is

$$E = \sum_{i=1}^{N_t} \left(S_i(n_A, V) - F_i \right)^2 \tag{B1}$$

where N_t is the number of data points, $S_i(n,V)$ and F_i are the simulated and reference concentrations, for example of F-actin at the time t_i (i-th data point).

As the values of n_A and V are finite, any estimation of the sum of squared residuals E is a random variable. We estimate the expected value of E using Eq. B2.

$$\left\langle E \right\rangle_{M \to \infty} = \frac{1}{M} \sum_{m=1}^{M} E_m = \frac{1}{M} \sum_{m=1}^{M} \sum_{i=1}^{N_t} \left(S_{im}(n_A, V) - F_{im} \right)^2 \tag{B2}$$

where M is the number of independent statistical experiments, E_m is the sum of squared residuals in the m-th statistical experiment. Manipulating with the summation order in Eq. B2 yields

$$\langle E \rangle_{M\to\infty} = \sum_{i=1}^{N_t}\left[\frac{1}{M}\sum_{m=1}^{M}\left(S_{im}(n_A,V) - F_{im}\right)^2\right] \tag{B3}$$

Noticing that the expression in the square brackets is the variation σ_i^2 of a residual at the i-th time point Eq. (B2) transforms into Eq. (B4). The expected value for the sum of squared residuals $\langle E \rangle_{M\to\infty}$ equals to the sum of variations in the time points N_t:

$$\langle E \rangle_{M\to\infty} = \sum_{i=1}^{N_t}\sigma_i^2 \tag{B4}$$

The problem of calculation of an approximation error is therefore converted to calculating the variations of the residuals at the selected time points. The simulated concentration $S_i(n,V)$, is a result of n_A simulations in the volume V, that is

$$S_i(n_A,V) = \frac{1}{n_A}\sum_{j=1}^{n_A} S_{ij}(V) \tag{B5}$$

Assume that the simulated volume V can be approximated by the k small independent minimal (critical) volumes V_{min}, $V = k * V_{min}$, the size of which is calculated from the estimation of a certain amount of protomers required to simulate a representative filament structure. Then, the simulated concentration $S_{ij}(V)$ is

$$S_{ij}(V) = \frac{N_{ij}}{V} = \frac{\sum_{l=1}^{k} N_{ijl}}{kV_{\min}} = \frac{1}{k}\sum_{l=1}^{k} s_{ijl} \tag{B6}$$

Where N_{ij} and N_{ijl} are the number of molecules in the volumes V and V_{min} respectively, $s_{ijl} = \sum_{l=1}^{k}\frac{N_{ijl}}{V_{\min}}$ is the simulated concentration of the F-actin in the l-th minimal volume V_{min}. Putting Eq. B6 into Eq. B5 gives

$$S_i(n_A,V) = \frac{1}{n_A}\sum_{j=1}^{n_A}\left(\frac{1}{k}\sum_{l=1}^{k} s_{ijl}\right) = \frac{1}{n_A k}\sum_{j=1}^{n_A}\sum_{l=1}^{k} s_{ijl} \tag{B7}$$

Recounting for the index $q = k(j-1)+l$ simplifies Eq. (B7) to

$$S_i(n_A,V) = \frac{1}{n_A k}\sum_{q=1}^{n_A k} s_{iq} \tag{B8}$$

Suppose that the simulated concentration s_{iq} for the minimal volume at the i-th time point is a normally distributed random variable, with mean F_i and variance $\hat{\sigma}_i^2$. Then, the estimation of the variance of the concentration in the volume V after n_A averaging at the i-th time point is

$$\sigma_i^2 = \frac{\hat{\sigma}_i^2}{n_A k} = \frac{\hat{\sigma}_i^2 V_{\min}}{n_A V} \tag{B9}$$

Combining Eq. (B4) and Eq. (B9) yields

$$\langle E \rangle_{M\to\infty} = \frac{V_{\min}}{n_A V} \sum_{i=1}^{N_t} \hat{\sigma}_i^2 \ . \tag{B10}$$

For the given system V_{min} is constant, and, therefore, the expected value of the sum of squared residuals E is inversely proportional to n_A and V.

To control the computational efficiency of the developed models, we take the simulation time T, that is the time spent by a PC to compute a model in the "virtual" time range $[t_0, t_{\max}]$. Evidently, on the one hand, the simulation time T is a linear function of the number of simulations $T = \alpha \cdot n_A$, where α is a constant coefficient of proportionality. On the other hand, the simulation time T should be a function of the simulated volume V. We checked the dependence between V and T on two representative examples of actin polymerization systems: i) the actin polymerization and ii) full-reactant assay, except the Arp2/3 complex, in terms of the nSRF model. The corresponding results are shown in Fig. S5 B. We observed a nonlinear dependence between the simulation time T and the simulated volume V that can be well fitted using Eq. (B11).

$$T = \gamma \cdot V^2 + \beta \cdot V \tag{B11}$$

where γ, β are constants, coefficients of proportionality. It is well known [4] that the computational cost of the Gillespie's direct method depends linearly on the number of reactions present in the system, that, in turn, are proportional to the simulated volume V, as is evident from the Eqs. (1) and (2), Manuscript. We justify the nonlinear computational cost as the consequence of the filament structure simulation. It algorithmically resulted from the procedure of searching a specific filament, for example, the filaments with ATP actin on the barbed end for the simulation of the reaction DITB (Table 1). We estimated the computational time of latter search that is proportional to the total number of filaments, i.e. to the volume V, and a sum of other minor calculations independent on the volume. Therefore, the total simulation time is the product of the computational costs required for simulating the bulk of reaction events and specific filament structures and searches.

Eqs. (B10) and (B11) indicate that an increase in n_A is computationally more efficient than expanding the V to minimize the computational time for the desired approximation error E.

Analytical models for actin polarization systems

Actin polymerization system. An analytical model of a pure actin system can mathematically be described by a balanced set of ordinary differential equations for changes in concentrations of reagents. This model can be used to interpret a simple system and to validate a simulation model (which can be used further for more complex systems). A similar analytical approach for the evaluation of filamentous actin kinetics was reported in [5]. In several reports [6, 7] equations were derived to study the nucleotide profile in the steady-state actin cycle (changes in concentrations were equated to zero).

The aging (ATP-hydrolysis) is not considered in this analytical model. To include it, the nucleotide profile of filaments, dynamically changed with time, must be developed.

The analytical model integrates as reagents: actin monomers (ATM), actin protomers (ATF), barbed ends (FTB) and pointed ends (FDB). Taking in account that [ATF] + [ATM] = A = *const* and [FTB] = [FDB], there are two linearly independent variables in this system, for example, [ATF] and [FTB]. The reagents participate in five biochemical reactions: spontaneous nucleation, associations at barbed and pointed ends and dissociations at barbed and pointed ends (*cf.* Table 1, Manuscript). The resulting set of differential equations is:

$$\begin{cases} \dfrac{d[ATF]}{dt} = 3k_{SNUC}\left(A-[ATF]-\dfrac{k_{DITB}}{k_{ASTB}}\right)^3 + k_{ASTB}[FTB]\left(A-[ATF]-\dfrac{k_{DITB}}{k_{ASTB}}\right)+ \\ \qquad + k_{ASTP}[FTB]\left(A-[ATF]-\dfrac{k_{DITP}}{k_{ASTP}}\right) \\ \dfrac{d[FTB]}{dt} = k_{SNUC}\left(A-[ATF]-\dfrac{k_{DITB}}{k_{ASTB}}\right)^3 \end{cases}, \quad \text{(C1)}$$

where $A=[ATF]+[ATM]$ is the total concentration of actin monomers and protomers. The ratios k_{DITB}/k_{ASTB} and k_{DITP}/k_{ASTP} are the critical concentrations of actin monomers for barbed and pointed ends respectively. The critical concentration of barbed ends can be used in the nucleation part of the equations to approximate an effect of short filaments dissociations [5].

Actin and capping protein. The second analytical model considers the same reagents as in a pure actin system plus free and bound barbed-end capping proteins ((CBM) and (CBF)). Three additional reactions are included: nucleation by barbed end capping protein, capping of barbed end and uncapping of barbed end. The number of active pointed and barbed ends differs in this situation. This system, combining six reagents and eight reactions, is described by a set of three linearly independent differential equations C2, if: i) the total actin concentration is constant, [ATF] + [ATM] = *A* = *const*; ii) the total concentration of barbed end capping protein is constant, $[CBF]+[CBM]=C=const$; iii) the equality for total concentrations of barbed and pointed ends is $[FTP]=[FTB]+[CBF]$.

$$\begin{cases} \dfrac{d[ATF]}{dt} = 3k_{SNUC}\left(A-[ATF]-\dfrac{k_{DITB}}{k_{ASTB}}\right)^3 + 3k_{CBNU}\left(A-[ATF]-\dfrac{k_{DITB}+k_{DITP}}{k_{ASTB}+k_{ASTP}}\right)^3 (C-[CBF])+ \\ + k_{ASTB}[FTB]\cdot\left(A-[ATF]-\dfrac{k_{DITB}}{k_{ASTB}}\right) + k_{ASTP}([FTB]+[CBF])\left(A-[ATF]-\dfrac{k_{DITP}}{k_{ASTP}}\right) \\ \dfrac{d[FTB]}{dt} = k_{SNUC}\left(A-[ATF]-\dfrac{k_{DITB}}{k_{ASTB}}\right)^3 - k_{ASCB}[FTB](C-[CBF])+k_{DICB}[CBF] \\ \dfrac{d[CBF]}{dt} = k_{CBNU}\left(A-[ATF]-\dfrac{k_{DITB}+k_{DITP}}{k_{ASTB}+k_{ASTP}}\right)^3 (C-[CBF])+k_{ASCB}[FTB](C-[CBF])-k_{DICB}[CBF] \end{cases} \quad \text{(C2)}$$

The ratios k_{DITB}/k_{ASTB} and k_{DITP}/k_{ASTP} are the critical concentrations of actins for barbed and pointed ends respectively. The critical concentration of barbed ends can be used in the actin nucleation part of the equations to approximate an effect of short filaments dissociations [5]. The ratio $(k_{DITB}+k_{DITP})/(k_{ASTB}+k_{ASTP})$ can be used in the barbed end capping protein nucleation part of the equations to approximate an effect of short capped filaments dissociations.

The differential equations C1 and C2 were solved numerically using Mathematica 6.

Software package *ActinSimChem*

ActinSimChem is the stand-alone software package for the Monte Carlo simulation of actin polymerization processes. *ActinSimChem* integrates the nSRF and SRF models (switching between two models is optional). *ActinSimChem* provides the possibility for: i) input/variation of the model parameters; ii) simulation of actin polymerization; iii) graphical representation of simulation results; iv) storage of the results. The program and its manual can be obtained on request or can be downloaded from the website http://actinsim.uni.lu.

The *ActinSimChem* is designed as a simple network of bound object-oriented classes (*cf.* Fig. S6):

- class *CSimpleCell* is an abstract parent class, in which the numbers of molecules for reagents are stored and the methods of stochastic chemical reactions simulations are implemented (the "direct" method, the "first reaction" method [4], the "next reaction" method [2]). The functions of the class operate by a list of 21 reagents in the same way for both nSRF and nSRF models. Procedures, which perform changes in the simulated system, are abstract in this class and are realized further in the child classes.
- Class *CCell* is the child class to the *CSimpleCell* class that implements the nSRF model. The corresponding procedures control filaments, filament branches, and the numbers of molecules for reagents according the nSRF model. Classes *CFilament* and *CFilBranch* are used to describe filaments and filament branches correspondingly.
- Class *CCellStruct* is the child of the class *CSimpleCell* that employs the SRF model. The corresponding procedures perform modifications of filaments, filament branches, and the number of molecules for reagents according the SRF model. Classes *CFilamentStruct* and the *CFilBranchStruct* are used to define filaments and filament branches correspondingly.
- Class *CFilament* is required for definition of a filament in the nSRF model. The filament is represented by the number of proteins, branch units, and by a pointer to the first branch unit.
- Class *CFilamentStruct* is used for description of a filament in the SRF model. The filament is represented by the number of proteins, branch units, and by a pointer to the first branch unit.
- Class *CBranch* is utilised for description of a 'daughter' filament or a branch in the nSRF model. A branch is represented by the number of proteins, types of barbed and pointed ends. The class *CFilBranch* is a child class to the *CBranch* that defines a pointer to the filament unit, a pointer to the 'mother' branch unit, pointers to the 'daughter' branch units, and that manages branch structures in the nSRF model.
- Class *CFilBranchStruct* is used for definition of a 'daughter' filament or a branch in the SRF model. Type and positions of proteins in filament branch are stored as a sequence of elements. The class *CElement* defines subunit. The class *CFilBranchStruct* is a child class to the *CBranchStruct* that contains a list of pointers to the 'daughter' branch units, a pointer to the 'mother' branch unit, a pointer to the filament unit, a position of the branch unit relative to pointed end of the 'mother' branch.
- Class *CElement* is needed to manage filament subunits in the SRF model. In particular, type of protein (ATF, APF, ADF, CBF, CPF, FOF, ARF) and the links to the next and previous elements in the filament branch are stored.

ActinSimChem was developed using the C++ Builder 2007.

REFERENCES

[1] S. Romero, C. Le Clainche, D. Didry, C. Egile, D. Pantaloni, M.F. Carlier, Formin is a processive motor that requires profilin to accelerate actin assembly and associated ATP hydrolysis, Cell 119 (2004) 419-429.

[2] M.A. Gibson, J. Bruck, Efficient exact stochastic simulation of chemical systems with many species and many channels, J. Phys. Chem. A 104 (2000) 1876-1889.

[3] Y. Cao, H. Li, L. Petzold, Efficient formulation of the stochastic simulation algorithm for chemically reacting systems, J Chem Phys 121 (2004) 4059-4067.

[4] D.T. Gillespie, A general method for numerically simulating the stochastic time evolution of coupled chemical reactions, J. Comput. Phys. 22 (1976) 403-434.

[5] A.E. Carlsson, M.A. Wear, J.A. Cooper, End versus side branching by Arp2/3 complex, Biophysical journal 86 (2004) 1074-1081.

[6] E.B. Stukalin, A.B. Kolomeisky, ATP hydrolysis stimulates large length fluctuations in single actin filaments, Biophysical journal 90 (2006) 2673-2685.

[7] M. Bindschadler, E.A. Osborn, C.F. Dewey, Jr., J.L. McGrath, A mechanistic model of the actin cycle, Biophysical journal 86 (2004) 2720-2739.

[8] J. Fass, C. Pak, J. Bamburg, A. Mogilner, Stochastic simulation of actin dynamics reveals the role of annealing and fragmentation, Journal of theoretical biology 252 (2008) 173-183.

[9] F.J. Brooks, A.E. Carlsson, Actin polymerization overshoots and ATP hydrolysis as assayed by pyrene fluorescence, Biophysical journal 95 (2008) 1050-1062.

CAPTIONS FOR FIGURES

Fig. S1. Testing the model for annealing and fragmentation of actin filaments.

(A) Examples of predicted average lengths of actin filaments for total actin concentrations $[ATM]_{t=0}$ = 2.0 μM (*solid*), 4.0 μM (*dashed*), and 6.0 μM (*dash-dot*) including normal fragmentation and annealing events. The *Inset* represents the steady state length distributions for simulations with 4.0 μM total actin both with and without normal fragmentation and annealing (*black bars* and *grey bars*, respectively). (B) Predicted average lengths of actin filaments for actin concentrations $[ATM]_{t=0}$ = 2.0 μM (*solid*) and 4.0 μM (*dashed*) with (*black color*) and without (*grey color*) normal fragmentation and annealing. $k_{FRGM} = 1.8\text{x}10^{-8}$ s^{-1}, $k_{ANNL} = 0.10$ $\mu M^{-1}s^{-1}$. Other reaction rates are the same as listed in Table 1, Manuscript.

Fig. S2. Testing the model for the occurrence of overshoots in the concentration of polymerized actin.

Examples of time series for predicted actin polymerization kinetics for three systems of initial actin concentration $[ATM]_{t=0}$ =3.0 μM: (i) actin {$k_{DTOT} = 20$ s^{-1}} (–♦–), (ii) actin in the absence of excess ATP {$k_{DTOT} = 0$ s^{-1}} (–▲–), and (iii) actin in the absence of excess ATP with Arp2/3 complex-induced branching included {$k_{DTOT} = 0$ s^{-1}, $[ARM]_{t=0}$=0.01 μM, $k_{ASRT} = 10^{-5}$ $\mu M^{-1}s^{-1}$, $k_{DIRP} = 10^{-3}$ s^{-1}} (–●–). Other reaction rates are the same as listed in Table 1, Manuscript.

As is reported previously, several mechanisms of actin polymerization may yield overshoots, for example, the absence of excess ATP, Arp2/3 complex-induced branching, severing, etc. [9]. We reproduced some of these overshoots. The maximum overshoot was observed for the actin system with an absence of excess ATP, resulting in the overshoot magnitude of $\Delta = F_{max} - F_{min} = ([ATM]_{t=0} - C_c^{B,T}) - ([ATM]_{t=0} - C_c^{B,D}) \approx 1.7$ μM, where F_{max} and F_{min} are maximum and minimum steady state limits at the actin polymerization curve, $C_c^{B,T}$ and $C_c^{B,D}$ are the ATP- and ADP-actin critical concentrations at the barbed end. Polymerization overshoot became faster ($k_{DTOT} = 0$ s^{-1}) or enhanced ($k_{DTOT} = 0.01$ s^{-1}, data not shown) as high concentration of Arp2/3 complexes (> 0.1 μM) were included in simulation. No overshoot was observed for a high nucleotide exchange rate ($k_{DTOT} = 20$ s^{-1}) as is in presence of profilin.

Fig. S3. nSRF (○) and SRF (♦) models differ when considering Arp2/3-complex dependent actin filament branching.

Decrease of the average filament length $\langle L \rangle$ in the steady-state phase with increasing concentration of the Arp2/3 complex and its nucleation activity at ATF-protomers in a 'mother' filament. $[ATM]_{t=0}$=3.0 μM, $[CBM]_{t=0}$=$[CPM]_{t=0}$=0.01 μM, $k_{SNUC} = 10^{-8}$ $\mu M^{-2}s^{-1}$, $k_{CBNU} = k_{CPNU} = 10^{-5}$ $\mu M^{-3}s^{-1}$, $k_{ASRT} = 10^{-2}$ $\mu M^{-1}s^{-1}$, $k_{DIRP} = 10^{-3}$ s^{-1}, $k_{FRGM} = 1.8\text{x}10^{-8}$ s^{-1} $k_{ANNL} = 10^{-8}$ $\mu M^{-1}s^{-1}$. If a parameter is not mentioned specifically, the value from Table 1 is used.

Fig. S4. Sensitivity of actin systems to the concentrations of capping proteins and various rate constants.

Plots (A-D) show the sensitivity of the system to barbed-end (A, C) and pointed-end (B,D) capping proteins. Spontaneous nucleation: $k_{SNUC} = 10^{-9}$ $\mu M^{-2}s^{-1}$, squares, circles, triangles and diamonds correspond to capping protein concentrations of 1, 0.1, 0.01, and 0.001 μM respectively.

(A) Sensitivity to [CBM] working as a nucleator ($k_{CBNU} = 2\text{x}10^{-5}$ $\mu M^{-3}s^{-1}$), $[ATM]_{t=0}$ = 2 μM.

(B) Sensitivity to [CPM] working as a nucleator ($k_{CPNU} = 2\text{x}10^{-5}$ $\mu M^{-3}s^{-1}$), $[ATM]_{t=0}$ = 2 μM.

(C) Sensitivity to [CBM], when it does not works as a nucleator ($k_{CBNU} = 0$), $[ATM]_{t=0}$ = 6 μM.

(D) Sensitivity to [CPM], when it does not works as a nucleator ($k_{CBNU} = 0$), $[ATM]_{t=0}$ = 6 μM.

Plots (E-H) show the sensitivity of the system to the rates. In all plots the pure actin system was considered, with the same actin concentration $[ATM]_{t=0}$ = 6 μM.

(E) and (F) represents the effect of actin exchange at barbed and pointed ends respectively. Circles correspond to the experimentally determined exchange rates (see Table 1, reactions of elongation and dissociations). Lines with squares have been obtained for the case, when these rates are multiplied by 2, and triangles when they are divided by 2.

(G) Sensitivity of the actin system to the spontaneous nucleation rate. Squares, circles, triangles and diamonds corresponds to k_{SNUC} of $15\text{x}10^{-9}$, $10\text{x}10^{-9}$, $5\text{x}10^{-9}$, 10^{-9} $\mu M^{-2}s^{-1}$.

(H) Sensitivity of the actin system to effect of the actin aging in filaments. Circles correspond to $k_{TTOD} = 7\text{x}10^{-4}$ s^{-1}, squares to $k_{TTOD} = 0.7$ s^{-1}.

Fig. S5. Comparison of different stochastic simulation schemes and computational efficiency.

(A) Comparison of the times spent for simulations by three stochastic simulation algorithms. White bars correspond to the Gillespie's "first reaction" algorithm, gray bars to "direct" Gillespie's algorithm and striped bars to a partially realized Gibson-Bruck's algorithm.

(B) Simulation time increase in relation to the volume V of simulated systems (i.e. number of simulated events). Circles represent timing obtained for simulation of the actin polymerization system whereas triangles represent a simulation with the complete reaction and reagent set (excluding the Arp2/3 complex and its reactions). Solid and dashed curves resulted from the fits by an approximating regression $T = \alpha \cdot V^2 + \beta \cdot V$, where α and β are the fitted constants.

Fig. S6. The network of the object-oriented classes in the program *ActinSimChem*. Class *CSimpleCell* is the abstract class that contains a stochastic simulation algorithm. Class *CElement* holds filament subunits in the SRF model. Classes *CFilament* and *CFilamentStruct* realize a model component of a filament in the nSRF and SRF models correspondingly. Classes *CFilBranch* and *CFilBranchStruct* are used to describe a filament branch in the nSRF/SRF models. Classes *CCell* and *CCellStruct* perform simulations according the nSRF and SRF models.

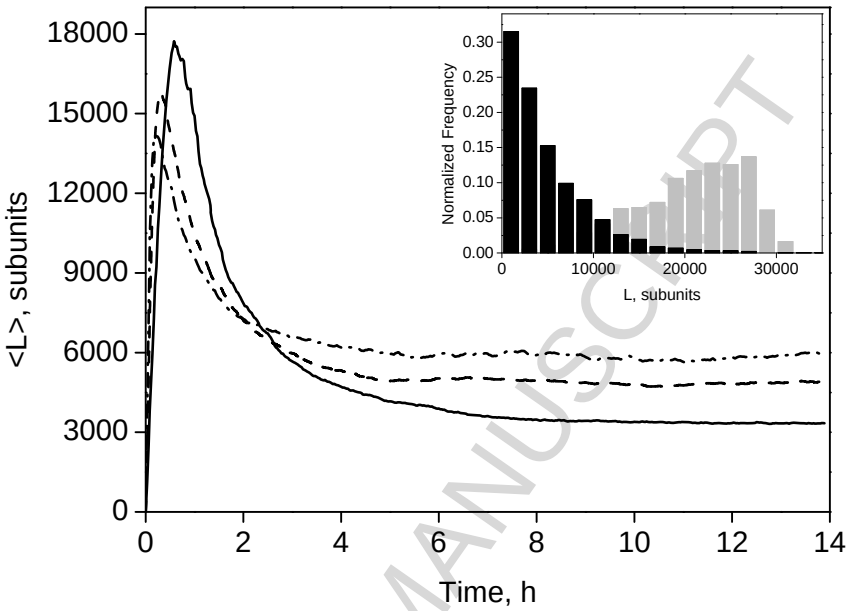

A

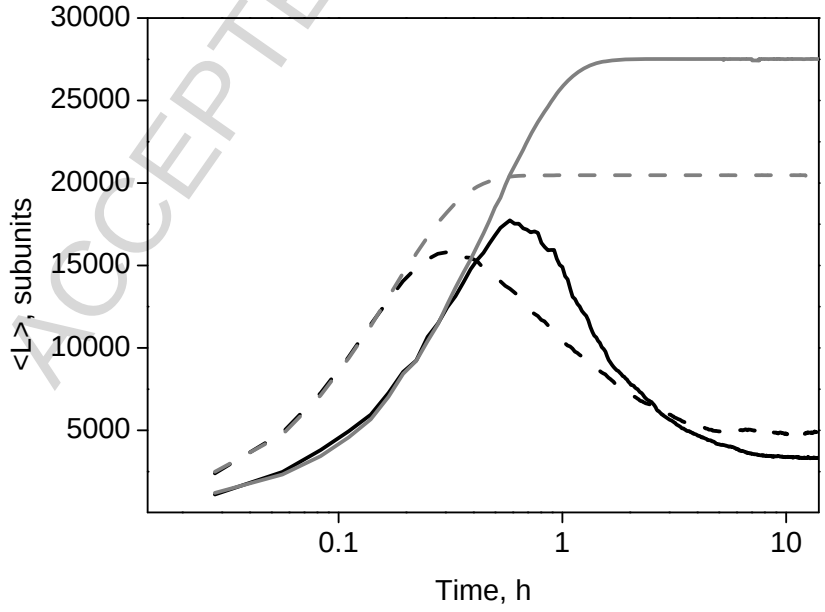

B

Fig. S1

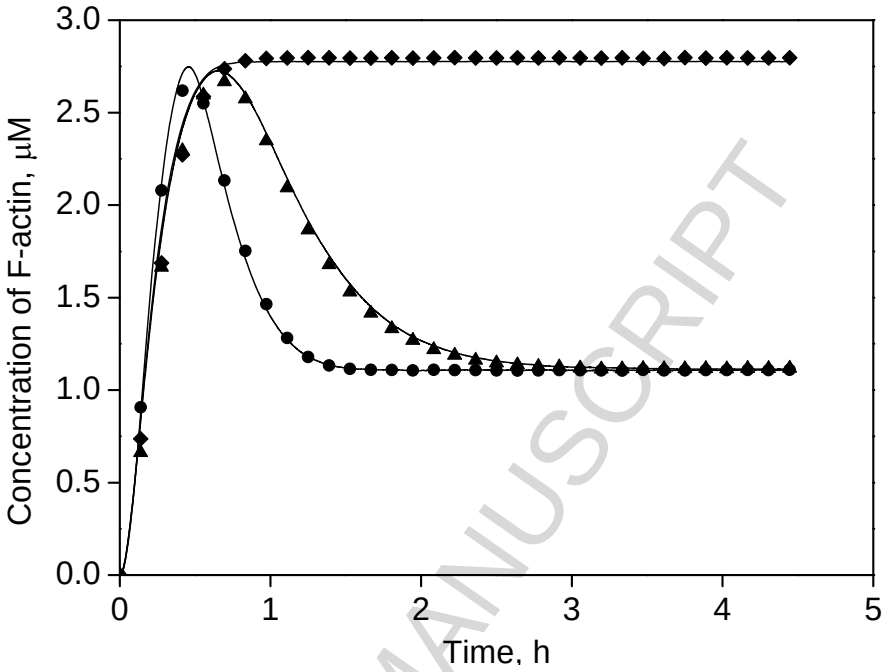

Fig. S2

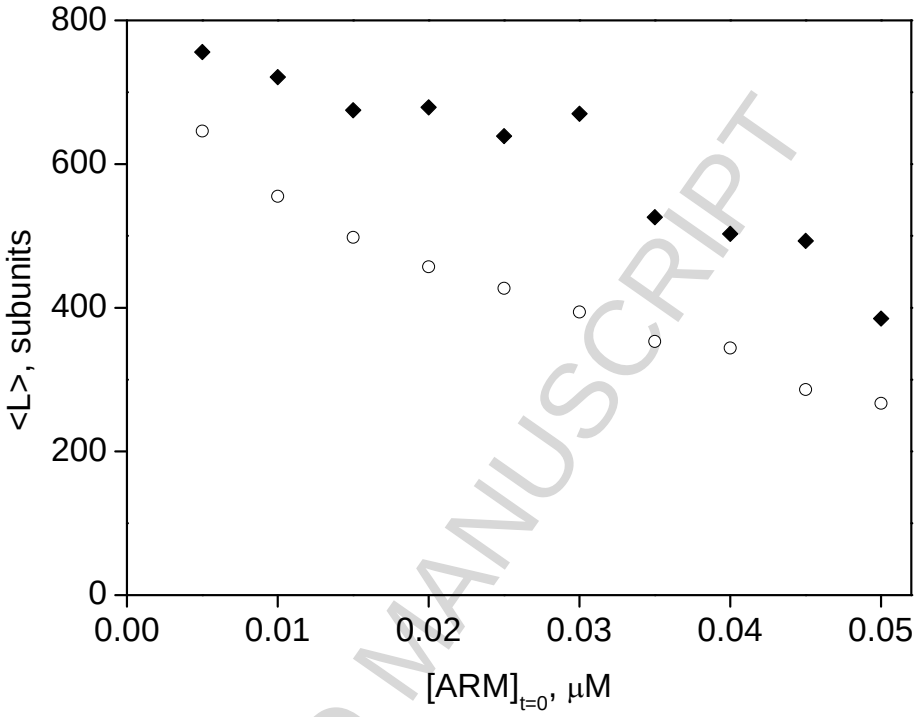

Fig. S3

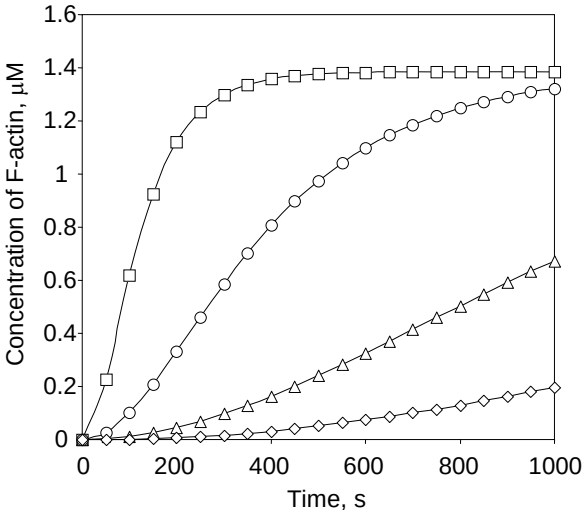

A

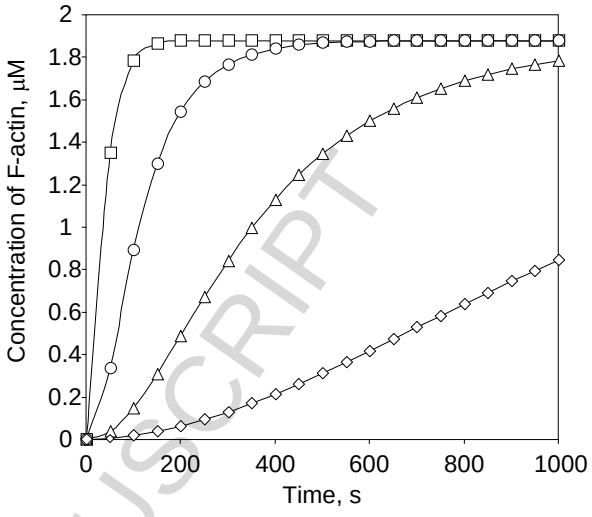

B

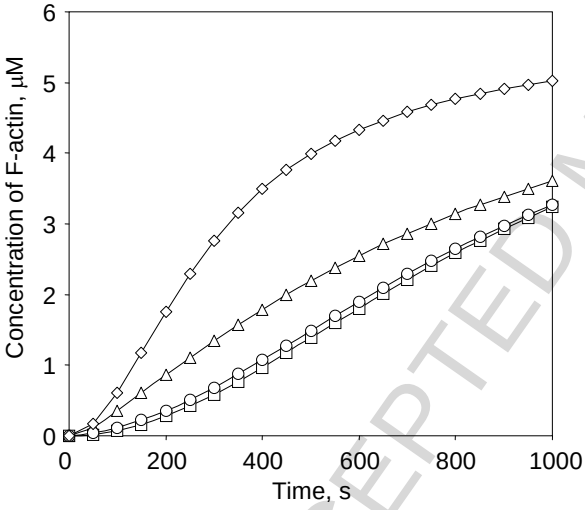

C

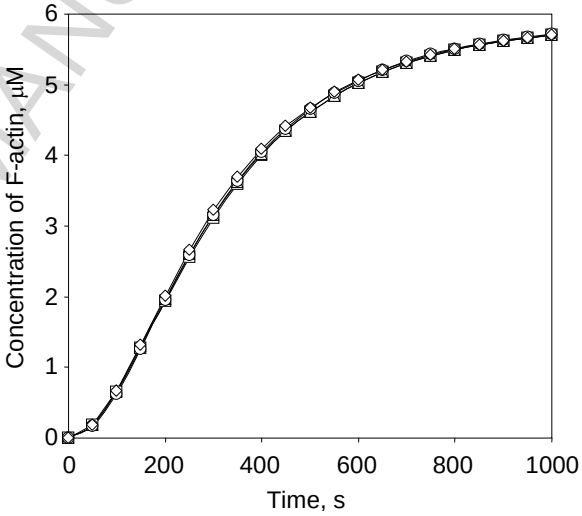

D

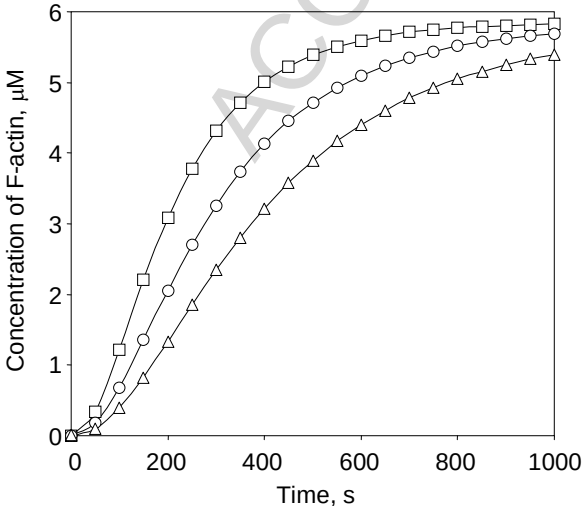

E

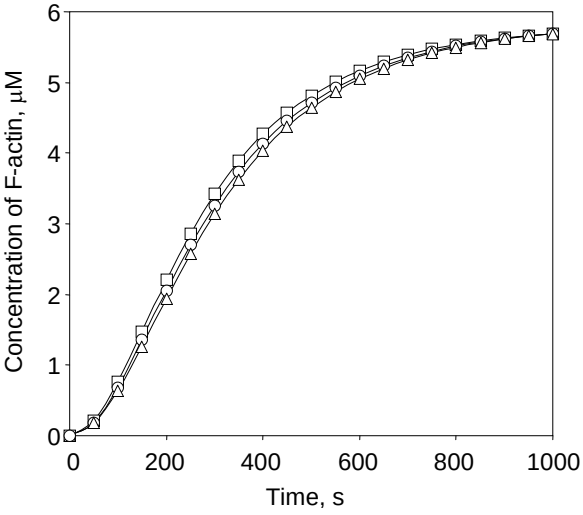

F

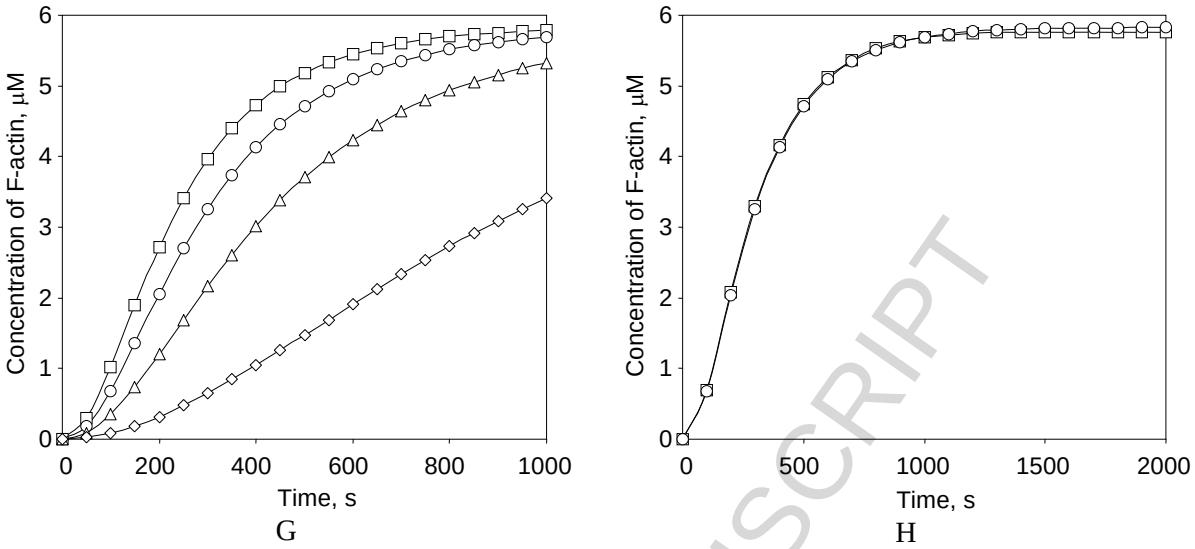

Fig. S4

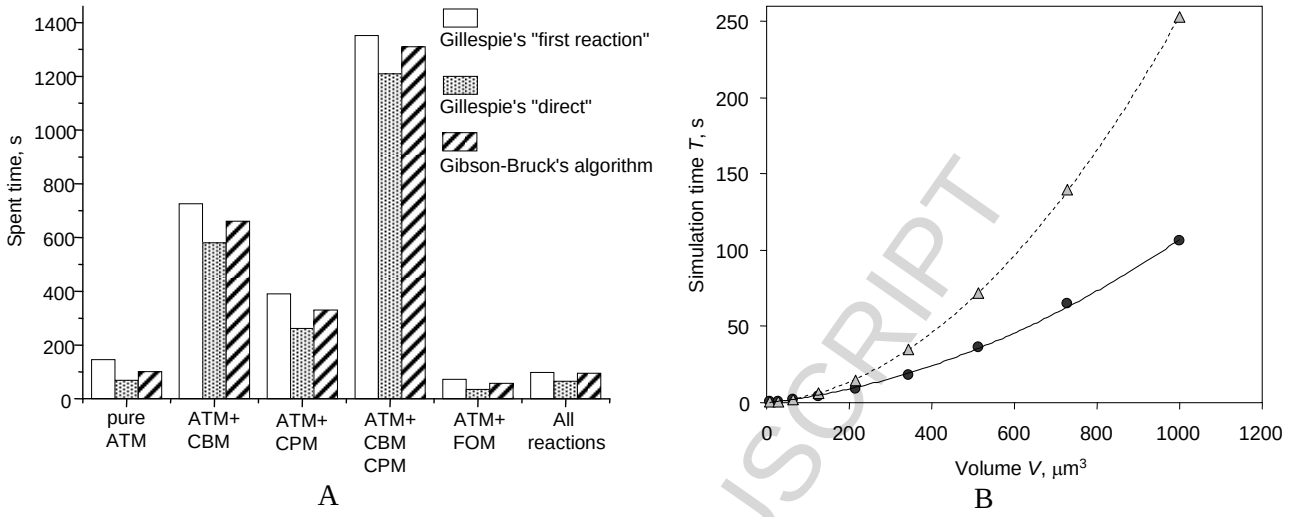

Fig. S5

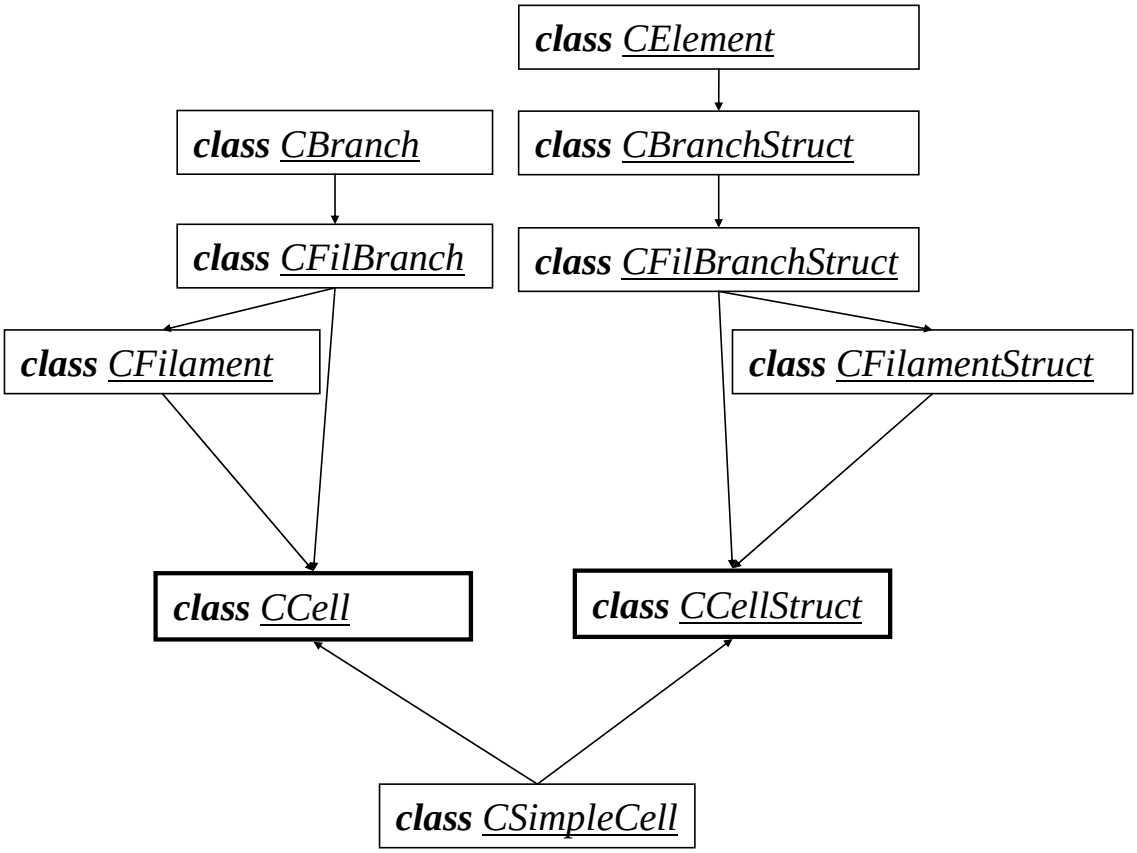

Fig. S6

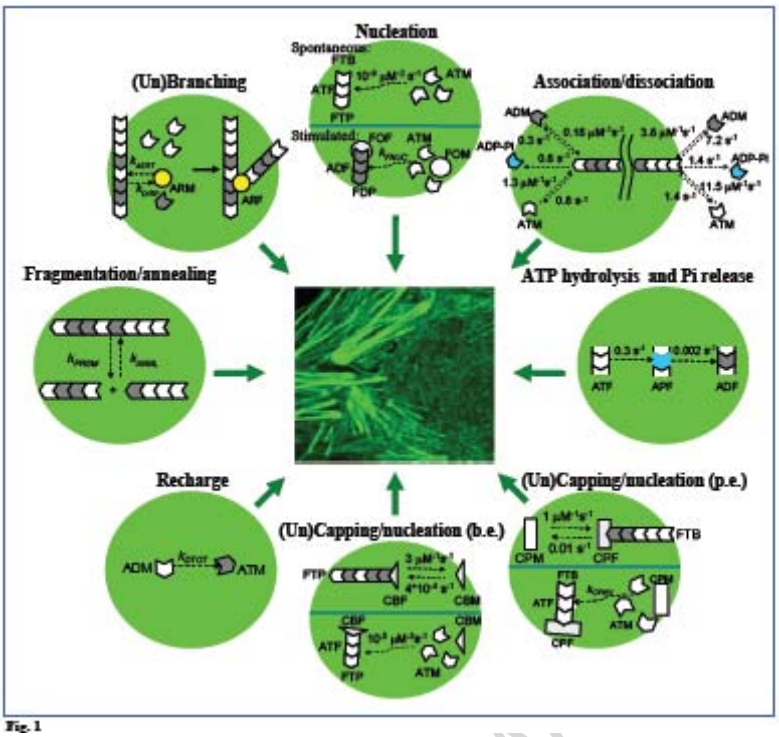

Fig. 1

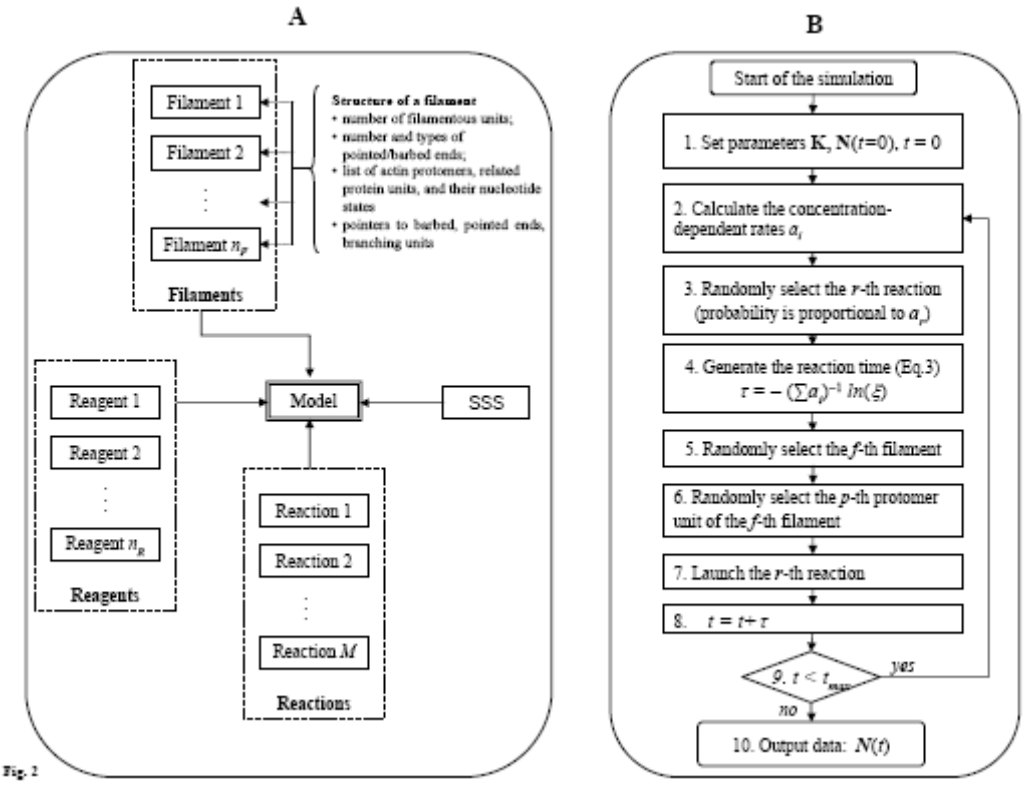

Fig. 2

Figure(s)

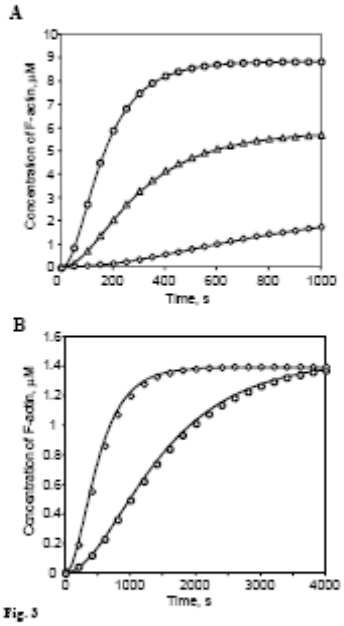

Fig. 3

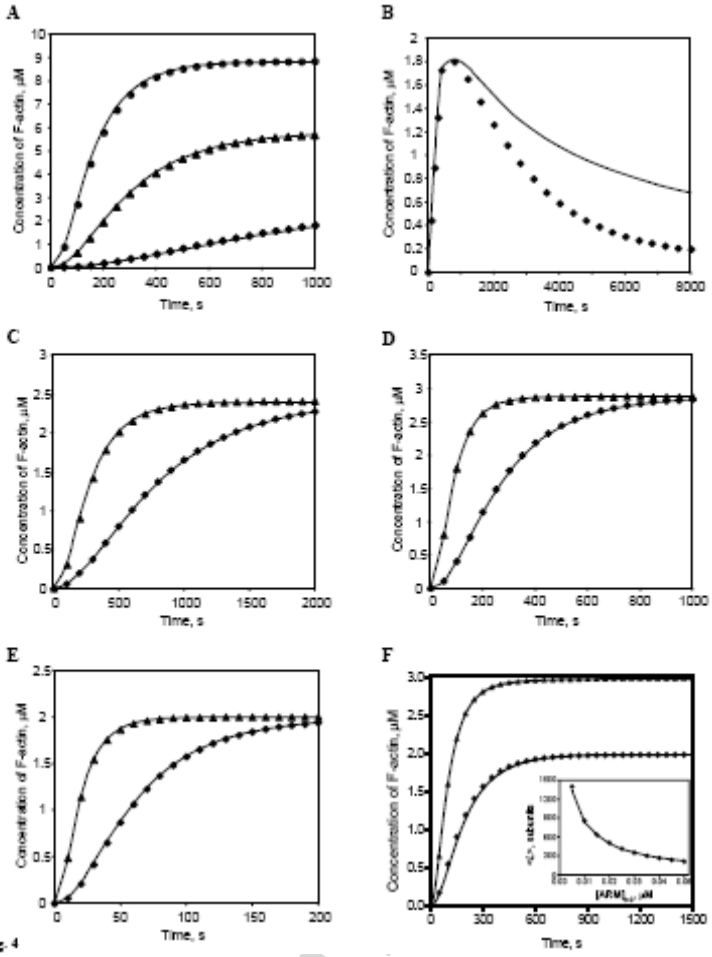

Fig. 4

Figure(s)

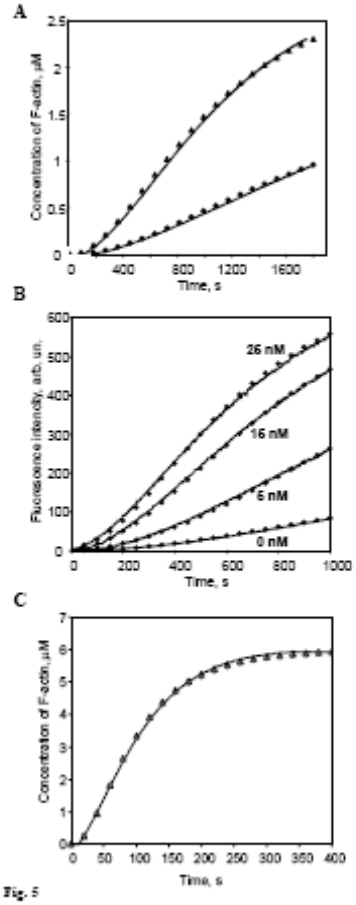

Fig. 5